UNIVERSITÀ DEGLI STUDI DI PISA

Facoltà di Scienze Matematiche, Fisiche e Naturali

Corso di Laurea Magistrale in Matematica

Tesi di Laurea

THE JUNO MISSION GRAVITY SCIENCE EXPERIMENT: A SEMI-ANALYTIC THEORY

Relatore:
Prof. ANDREA MILANI COMPARETTI

Candidato:
DANIELE SERRA

Controrelatore:
Dott. GIACOMO TOMMEI

ANNO ACCADEMICO 2011-2012

CONTENTS

LIST OF FIGURES

INTRODUCTION

Interplanetary space missions have been projected since the early 60s, when the Sovietic probe Venera 1 was launched and encountered planet Venus at a distance of 100000 km. Since then, more and more technologically advanced missions have been designed, all with the common aim to discover unknown features of the celestial bodies we know.

Juno is a NASA mission, part of the *New Frontiers* program, whose objective is the study of planet Jupiter by means of a spinning orbiter. The spacecraft has been launched from Cape Canaveral on August 5, 2011 and will arrive to Jupiter in 2016. At the arrival, it will be inserted in a high-eccentric polar orbit with a period of 11 days. If $R_{♃}$ is Jupiter's equatorial radius, the perijove will be $\simeq 1.06R_{♃}$ far from Jupiter's center of mass, while the apojove will be about $39R_{♃}$ distant. As effect of Jupiter's oblateness, the perijove latitude will increase in time. The nominal mission is composed of 32 orbits, for a duration of one year; during the perijove passages, the probe will collect plenty of datas which will be sent to Earth.

The *Gravity Science experiment* consists in the determination of Jupiter's gravity field, by means of Doppler tracking of the spacecraft, which will be performed by X-Band and Ka-Band trasponders communicating with the Deep Space Network in California during orbits 8 to 32. This experiment is essential to reveal Jupiter's interior structure, as it will help mapping the mass distribution inside the planet and constrain Jupiter's core mass. In order to make this possible, an essential requirement is that the gravity field must be determined with an a priori established uncertainty. It is therefore essential to make a preliminary study of the accuracy of the experiment.

The objective of this thesis is to develop a semi-analytic theory to study the uncertainty with which Jupiter's gravity field can be determined, depending on the geometry of the Juno probe's orbit.

We start describing the mathematical setting: we model a planet as a limited set $W \subseteq \mathbb{R}^3$, with associated a distribution of mass ρ. The *gravitational potential* of W is a real valued function $U\colon \mathbb{R}^3 \to \mathbb{R}$ such that $\operatorname{grad} U$ is the gravity field of the planet. Thus, determining the gravity field is equivalent to recovering the gravitational potential. It can be shown that U is a harmonic function on $\mathbb{R}^3 \setminus W$, therefore it can be expanded in series of spherical harmonics. Using spherical coordinates:

$$U = \frac{GM}{r}\left\{\sum_{\ell=0}^{\infty}\sum_{m=0}^{\ell} P_{\ell m}(\sin\theta)\frac{R_{\oplus}^{\ell}}{r^{\ell}}[C_{\ell m}\cos(m\lambda) + S_{\ell m}\sin(m\lambda)]\right\},$$

where $P_{\ell m}$ are the *Legendre's associated functions*, $R_{\oplus}$ is the radius of an open ball strictly containing W, $C_{\ell m}, S_{\ell m}$ are adimensional and are called *harmonic coefficients*. Thus, it

is sufficient to determine the harmonic coefficients to know the gravitational potential of a planet. After having carefully formalized the problem of computing these coefficients, relying on some classical methods of orbit determination such as least squares method, our attention focuses on the study of the uncertainty with which Jupiter's *zonal* harmonic coefficients $C_{\ell 0}$ can be determined by means of Juno mission.
The method we describe selects as observables the *range-rate* of the spacecraft, that is the component of the velocity of the spacecraft along the direction of the Earth. We show that a measurement of the range-rate corresponds to a direct measurement of the potential, and use this fact to give analytical formulæ for the normal matrix C. The uncertainty is obtained by the diagonal entries of the covariance matrix $\Gamma := C^{-1}$. We repeat this analysis twice: in the first instance we suppose the planet Jupiter being axial symmetric, which is equivalent to assume the correlations among the zonal coefficients and the *tesseral* harmonic coefficients $C_{\ell m}, S_{\ell m},\ m \neq 0$, being all zero; then, we take these correlations into account, that is we eliminate the axial symmetry hypothesis from for our model.
In the first case we also perform a principal components analysis: if $V^{(1)}, \dots, V^{(N)}$ are unit eigenvectors of the covariance matrix, relative to the eigenvalues $\lambda_1 > \cdots > \lambda_N > 0$, we map each $V^{(i)}$ onto a function $\mathcal{U}^{(i)}$, representing the contribute of the i-th semiaxis of the confidence ellipsoid to the surface acceleration uncertainty as function of the latitude θ of Jupiter. To consider the contributes all at once, we use the root mean square of $(\mathcal{U}^{(i)})_i$, indicated by $\mathcal{U}(\theta)$. By studying the function $\mathcal{U}(\theta)$, it is possible to predict in which regions of the planet the gravity field will be recovered more accurately.

The theoretical study is combined with a software implementation: we built a simple MATLAB function, called `uncertainties`, which executes the previously described analysis and plots the results. More specifically, it uses 25 simulated perijove passages of Juno spacecraft, corresponding to the ones destined to Gravity Science experiment, and computes the uncertainty of the first 40 zonal harmonic coefficients with and without the correlations with tesseral coefficients. Moreover, it plots the surface acceleration uncertainty $\mathcal{U}(\theta)$ as function of the latitude. The results we obtained are perfectly in accordance with the previsions: the gravity field looks well recovered only in the 11°N-34°N latitude belt, which corresponds to the latitudes of the perijove during the Gravity Science orbits.
We also compare our results with the numerical simulations carried on by the *Radio Science Laboratory* (University of Rome, "La Sapienza"): we find out the same qualitative behaviour, although our results are more optimistic. Some reasons for this diversity are analysed.

This thesis is structured as follows:

CHAPTER 1 It contains an introduction to orbit determination, as treated in [5], in which we recall the basic tools such as least squares method or the confidence ellipsoid, and we establish the notations.

CHAPTER 2 Following [5], [3] and [9], we deal with the gravity field of a planet, giving a mathematical definition of it and exploring its properties, such as the fundamental expansion in spherical harmonics.

CHAPTER 3 It is a brief overview on Juno mission, mainly based on [4], in which we describe the mission goals, mission design, the payload and the necessary operations which will ensure the success of the mission.

CHAPTER 4 It is the heart of the work, in which we study the uncertainty in the determination of Jupiter's gravity field; this chapter contains almost entirely original material.

This thesis ends with some cues for future research: as our results depend exclusively on the geometry of the orbit of the spacecraft, we can attempt to design and implement a software for the study of the uncertainty of *any planet* gravity field, using as input datas only the orbit of the probe. This could be an useful tool to be utilized in a preliminary phase of space mission planning to have indications on the errors that must be expected. Of course, this work must be anticipated by several studies and tests on past space missions to confirm our conjectures.

1

ORBIT DETERMINATION

Orbit determination dates back to XVIII century, when Gauss first proposed a method to determine the orbit of celestial bodies starting from some few observations. The tools provided by orbit determination not only allow to compute orbits, but also other parameters, such as the gravity field of a planet or some calibration parameters of an accelerometer. In this chapter we recall the topics about orbit determination we need to proceed with our exposition and introduce the notations we'll largely use throughout the work.

1.1 FORMULATION OF THE PROBLEM

We start with some definitions. Unless it's differently specified, we assume $\mathbb{R}^n$ is endowed with the standard scalar product.

DEFINITION 1.1 - Let $\mathbf{f}$: $\mathbb{R}^p \times \mathbb{R} \times \mathbb{R}^{p'} \to \mathbb{R}^p$ with some regularity; the *equation of motion* is a system of ordinary differential equations

$$\frac{d\mathbf{y}}{dt} = \mathbf{f}(\mathbf{y}, t, \boldsymbol{\mu}),$$

where $\mathbf{y}$ is the *state vector*, $\boldsymbol{\mu}$ the *dynamical parameters*, t the time. If t_0 is the starting instant, $\mathbf{y}_0 := \mathbf{y}(t_0)$ is the vector of the *initial conditions*.

EXAMPLE 1.2 - The vector of the dynamical parameters may include the gravitational potential coefficients and the state vector may hold the position and the velocity of the body.

We are interested in solving the Cauchy's problem made up of the previous ODE system and assigned initial conditions.

DEFINITION 1.3 - An *orbit* is a solution of an equation of motion.

We indicate an orbit by $\mathbf{y} = \mathbf{y}(\mathbf{y}_0, t, \boldsymbol{\mu})$, underlining its dependence upon the initial conditions, the dynamical parameters and the time, of course.

Together with orbits, observations are the main characters of orbit determination; with the next definition we give a formal description of it.

DEFINITION 1.4 - Let $\boldsymbol{\nu} \in \mathbb{R}^{p''}$ a vector of *kinematical parameters*; the *observation function* is a function $R(\mathbf{y}, t, \boldsymbol{\nu})$. The *prediction function* is the composition of the observation function and the orbit, that is

$$r(t) := R(\mathbf{y}(t), t, \boldsymbol{\nu}).$$

EXAMPLE 1.5 - The prediction function is used to predict the result of an observation: for example, if we wish to estimate the distance of a spacecraft from a ground station, we choose as R some suitable distance between two points.

Let us suppose we have m observations $r_1, \dots, r_m$ at times $t_1, \dots, t_m$. We estimate them with the predictions $r(t_1), \dots, r(t_m)$, but in general their difference is non zero. This difference plays a fundamental role in orbit determination.

DEFINITION 1.6 - The *residual* at time t_i is

$$\xi_i := r_i - r(t_i).$$

The vector of the residuals is $\boldsymbol{\xi} := (\xi_i)_i$, $i = 1, \dots, m$.

REMARK 1.7 - The vector $\boldsymbol{\xi}$ is function of the initial conditions $\mathbf{y}_0$, the dynamical parameters $\boldsymbol{\mu}$ and the kinematical parameters $\boldsymbol{\nu}$.

Orbit determination is used to perform a computation of the orbit of some observed celestial bodies, of course, but also dynamical or kinematical parameters can be estimated.

DEFINITION 1.8 - The vector of the *fit parameters* is a subvector $\mathbf{x} \in \mathbb{R}^N$ of the vector $(\mathbf{y}_0, \boldsymbol{\mu}, \boldsymbol{\nu})$.

The fit parameters are the ones we wish to determine, the others are called *consider parameters* and have to be treated as constants.
The idea of Gauss method is to define an appropriate function, depending upon the vector $\mathbf{x}$, whose minimization provides the solution. Such a function should have some good properties, for example it is desirable to choose some quadratic form of the residuals.

DEFINITION 1.9 - The *target function* is

$$Q(\boldsymbol{\xi}) := \frac{1}{m} \boldsymbol{\xi}^T \boldsymbol{\xi} = \frac{1}{m} \sum_{i=1}^{m} \xi_i^2.$$

We can consider the target function as dependent upon the fit parameters:

$$Q(\mathbf{x}) := Q(\boldsymbol{\xi}(\mathbf{x})).$$

In this notation, the minimum principle can be enounced as follows.

MINIMAL PRINCIPLE The *nominal solution* is the point $\mathbf{x}^* \in \mathbb{R}^N$ such that

$$Q^* := Q(\mathbf{x}^*) = \min_{\mathbf{x} \in V} Q(\mathbf{x}),$$

where $V \subseteq \mathbb{R}^N$ is a suitable set of feasible parameters.

1.2 LEAST SQUARES PROBLEM

1.2.1 *Linear least squares*

Let's suppose that the prediction function can be expressed as linear combination of N functions $\varphi_1, \dots, \varphi_N$, with the fit parameters as coefficients; if $\lambda_1, \dots, \lambda_m$ are the observations at times $t_1, \dots, t_m$, then the residuals are

$$\xi_i(\mathbf{x}) = \lambda_i - \sum_{j=1}^{N} x_j \varphi_j(t_i), \quad i = 1, \dots, m$$

and the target function is

$$Q(\mathbf{x}) = \frac{1}{m} \sum_{i=1}^{m} \left[\lambda_i - \sum_{j=1}^{N} x_j \varphi_j(t_i) \right]^2.$$

By defining the *design matrix*

$$B = (b_{ij}) := \left(\frac{\partial \xi_i}{\partial x_j} \right)$$

and remarking that $b_{ij} = -\varphi_j(t_i)$, the target function can be rewritten as

$$Q(\mathbf{x}) = \frac{1}{m}(\boldsymbol{\lambda} + B\mathbf{x})^T(\boldsymbol{\lambda} + B\mathbf{x}) = \frac{1}{m}(\boldsymbol{\lambda}^T\boldsymbol{\lambda} + 2\boldsymbol{\lambda}^T B\mathbf{x} + \mathbf{x}^T B^T B\mathbf{x}).$$

By the minimum principle, the nominal solution is the solution of the following linear system:

$$m\frac{\partial Q}{\partial \mathbf{x}} = 2(\boldsymbol{\lambda}^T B + \mathbf{x}^T B^T B) = \mathbf{0}.$$

DEFINITION 1.10 - The matrix $C := B^T B$ is called *normal matrix*. If we define $D := -B^T\boldsymbol{\lambda}$, the *normal equations* are

$$C\mathbf{x} = D, \tag{1.1}$$

which provide the nominal solution $\mathbf{x}^*$. If C is full-rank, its inverse Γ is called *covariance matrix* and the previous equation is equivalent to

$$\mathbf{x}^* = -\Gamma D.$$

REMARK 1.11 - The normal matrix is symmetric and positive semidefinite; it defines a non-negative quadratic form on $\mathbb{R}^N$ by

$$q(\mathbf{x}) := \mathbf{x}^T C \mathbf{x}.$$

With this definition, we can compare two symmetric, positive semidefinite matrices: let C_1, C_2 be two such matrices and q_1, q_2 the associated quadratic forms; we say that

$$C_1 < C_2 \text{ if } q_1(\mathbf{x}) < q_2(\mathbf{x}) \text{ for all } \mathbf{x} \in \mathbb{R}^N.$$

1.2.2 *Non linear least squares*

In the most general case, the residual is a non linear function of the fit parameters and the target function

$$Q(\mathbf{x}) = \frac{1}{m} \sum_{i=1}^{m} \xi(\mathbf{x})^T \xi(\mathbf{x})$$

is no more a quadratic function, but it's still differentiable. We can define the design matrix as before:

$$B := \frac{\partial \xi}{\partial \mathbf{x}} = \left(\frac{\partial \xi_i}{\partial x_j} \right)$$

and the three-index array of the second derivatives:

$$H := \frac{\partial^2 \xi}{\partial \mathbf{x}^2}.$$

Again by the minimum principle, we should solve

$$\frac{\partial Q}{\partial \mathbf{x}}(\mathbf{x}) = \frac{2}{m} \xi^T B = 0 \tag{1.2}$$

to obtain the nominal solution, but this time the preceeding equation is a non-linear system, which may not admit any solution or may have many.

1.2.3 *Numerical methods*

From a numerical point of view, an iterative method is suitable to solve the (1.2). We have two ways to achieve this aim:

NEWTON'S METHOD It defines a sequence $(\mathbf{x}_k)_k$ such that

$$\begin{aligned} \mathbf{x}_{k+1} &= \mathbf{x}_k - \left[\frac{\partial^2 Q}{\partial \mathbf{x}^2}(\mathbf{x}_k) \right]^{-1} \frac{\partial Q}{\partial \mathbf{x}}(\mathbf{x}_k) \\ &= \mathbf{x}_k - (B^T B + \xi^T H)^{-1} B^T \xi, \end{aligned}$$

where the matrices B and H are computed at $\mathbf{x}_k$. The convergence of this method heavily depends upon the choice of the initial guess $\mathbf{x}_0$.

DIFFERENTIAL CORRECTIONS This method is obtained from Newton method by negelecting the terms containing the second derivatives H. The iteration is

$$\begin{aligned}\mathbf{x}_{k+1} &= \mathbf{x}_k - (B^T B)^{-1} B^T \xi \\ &= \mathbf{x}_k + \Gamma D,\end{aligned}$$

where Γ, D are evaluated at $\mathbf{x}_k$. If C is not invertible, each iteration of the differential corrections requires the solution of the linear least squares problem

$$C(\mathbf{x}_{k+1} - \mathbf{x}_k) = D.$$

1.2.4 *Weighted least squares*

Considering a different non-negative quadratic form as target function is not forbidden. The reasons leading to this generalization are many: for example, we may want to assign more importance to one observation rather than to another, or simply we want to express the residuals in some appropriate unit.

DEFINITION 1.12 - A *weight matrix* is a symmetric positive semidefinite matrix $W \in \mathbb{R}^{N\times N}$. The *weighted least squares problem* is defined by the target function

$$Q(\xi) := \frac{1}{m}\xi^T W \xi.$$

REMARK 1.13 - With this choice, the normal matrix is $B^T WB$ and the right side of the normal equation is $-B^T W\xi$.

Here we're going to analyze two cases, for a deeper argumentation see [5].

UNIFORM WEIGHT It's the case of $W := s^{-2}I$, corresponding to the change of scale. In this case $C = s^{-2}B^T B$ and $D = -s^{-2}B^T\xi$, therefore the normal equation is the same of non-weighted case, but the covariance matrix does change.

NON UNIFORM WEIGHT Choosing $W := \operatorname{diag}(s_1^{-2}, \dots, s_N^{-2})$, we are giving each observation a different importance. By normalizing the residuals, that is multiplying ξ_i by s_i^{-1}, we obtain a new residual ξ_i'; formulating the weighted least squares problem in terms of ξ', it's easy to see that we obtain the classical least squares problem.

1.3 CONFIDENCE ELLIPSOIDS

In this section we study the uncertainty of the solution of the least squares problem, by introducing a basic tool which helps us understanding how much the computed solution is good, that is how far from the nominal solution $\mathbf{x}^*$ it is.

DEFINITION 1.14 - Let Q be a target function of a least squares problem, Q^* its minimum value. For $\sigma > 0$, the *confidence region* at σ is the set

$$Z(\sigma) := \left\{ \mathbf{x} \in \mathbb{R}^N \mid Q(\mathbf{x}) \leqslant Q^* + \frac{\sigma^2}{m} \right\}.$$

The confidence region expresses the idea that the target function achieves its minimum at the nominal solution, but values of $\mathbf{x}$ such that $Q(\mathbf{x})$ is close to Q^* are still acceptable.

REMARK 1.15 - Let's define the *penalty* at $\mathbf{x} \in \mathbb{R}^N$ by $\Delta Q(\mathbf{x}) := Q(\mathbf{x}) - Q^*$. We can expand this penalty around $\mathbf{x}^*$:

$$\begin{aligned} \Delta Q(\mathbf{x}) &= \frac{1}{m}\frac{\partial Q}{\partial \mathbf{x}}(\mathbf{x}^*)^T(\mathbf{x}-\mathbf{x}^*) + \frac{1}{m}(\mathbf{x}-\mathbf{x}^*)^T\frac{\partial^2 Q}{\partial \mathbf{x}^2}(\mathbf{x}^*)(\mathbf{x}-\mathbf{x}^*) + O(|\mathbf{x}-\mathbf{x}^*|^3) \\ &= \frac{1}{m}(\mathbf{x}-\mathbf{x}^*)^T C(\mathbf{x}-\mathbf{x}^*) + O(|\mathbf{x}-\mathbf{x}^*|^3) + O(|\xi|)O(|(\mathbf{x}-\mathbf{x}^*)|^2). \end{aligned} \tag{1.3}$$

By the expansion above, we can approximate the confidence region by the confidence ellipsoid:

DEFINITION 1.16 - The *confidence ellipsoid* at $\sigma > 0$ is the set

$$Z_L(\sigma) := \left\{ \mathbf{x} \in \mathbb{R}^N \mid (\mathbf{x}-\mathbf{x}^*)^T C(\mathbf{x}-\mathbf{x}^*) \leqslant \sigma^2 \right\}.$$

REMARK 1.17 - The set $Z_L(\sigma)$ is indeed the interior of a $(N-1)$- dimensional ellipsoid if and only if C is positive definite.

Let's study the uncertainty of the parameters by means of the confidence ellipsoid. To do this, we split the vector $\mathbf{x}$ into two subvectors $\mathbf{g}, \mathbf{h}$, which are the projections of $\mathbf{x}$ along two orthogonal subspaces of $\mathbb{R}^N$:

$$\mathbf{x} = \begin{pmatrix} \mathbf{g} \\ \mathbf{h} \end{pmatrix}.$$

The design matrix results splitted, too:

$$B = (B_{\mathbf{g}}, B_{\mathbf{h}}) := \left(\frac{\partial \xi}{\partial \mathbf{g}}, \frac{\partial \xi}{\partial \mathbf{h}} \right),$$

therefore the normal matrix and the covariance matrix (if exists) have the following block form:

$$C = \begin{pmatrix} C_{\mathbf{gg}} & C_{\mathbf{gh}} \\ C_{\mathbf{hg}} & C_{\mathbf{hh}} \end{pmatrix}, \quad \Gamma = \begin{pmatrix} \Gamma_{\mathbf{gg}} & \Gamma_{\mathbf{gg}} \\ \Gamma_{\mathbf{hg}} & \Gamma_{\mathbf{hh}} \end{pmatrix}.$$

In this notation, the expansion (1.3) is equivalent to

$$\begin{aligned} m\Delta Q(\mathbf{x}) \simeq\ & (\mathbf{g}-\mathbf{g}^*)^T C_{\mathbf{gg}}(\mathbf{g}-\mathbf{g}^*) \\ & + 2(\mathbf{g}-\mathbf{g}^*)^T C_{\mathbf{gh}}(\mathbf{h}-\mathbf{h}^*) + (\mathbf{h}-\mathbf{h}^*)^T C_{\mathbf{hh}}(\mathbf{h}-\mathbf{h}^*). \end{aligned} \tag{1.4}$$

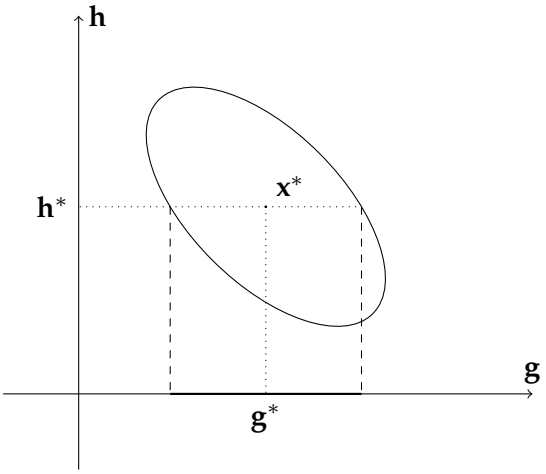

Figure 1.1.: Conditional confidence ellipsoid of $\mathbf{g}$ for $\mathbf{h} = \mathbf{h}^*$.

1.3.1 *Conditional ellipsoid for nominal values*

Let's fix $\mathbf{h}$ to the nominal value $\mathbf{h}^*$. Then the expansion (1.3) becomes

$$m\Delta Q(\mathbf{x}) \simeq (\mathbf{g} - \mathbf{g}^*)^T C_{\mathbf{gg}} (\mathbf{g} - \mathbf{g}^*),$$

defining an ellipsoid in the subspace of the $\mathbf{g}$ variables, called *conditional confidence ellipsoid* (see figure 1.1). This operation corresponds to selecting as fit parameters the subvector $\mathbf{g}$ and moving the others into the consider parameters.

REMARK 1.18 - The covariance matrix $C_{\mathbf{gg}}^{-1}$ is not equal to $\Gamma_{\mathbf{gg}}$, unless the correlations with $\mathbf{h}$ are zero, that is $C_{\mathbf{gh}} = C_{\mathbf{hg}} = 0$.

1.3.2 *Marginal ellipsoid*

Now we study the uncertainty of the $\mathbf{g}$ parameters for any value of the $\mathbf{h}$ parameters. Geometrically, it corresponds to project the confidence ellipsoid onto the $\mathbf{g}$ subspace (see figure 1.2). If the submatrix $C_{\mathbf{hh}}$ is invertible, the quadratic approximation of the expansion (1.3) becomes

$$m\Delta Q(\mathbf{x}) \simeq (\mathbf{g} - \mathbf{g}^*)^T C^{\mathbf{gg}} (\mathbf{g} - \mathbf{g}^*), \quad C^{\mathbf{gg}} = C_{\mathbf{gg}} - C_{\mathbf{gh}} C_{\mathbf{hh}}^{-1} C_{\mathbf{hg}},$$

defining the *marginal confidence ellipsoid*.

REMARKS 1.19
- It's easy to check that $C_{\mathbf{gh}} C_{\mathbf{hh}}^{-1} C_{\mathbf{hg}}$ is a symmetric semidefinite positive matrix; by remark 1.11, it follows that

$$C^{\mathbf{gg}} < C_{\mathbf{gg}},$$

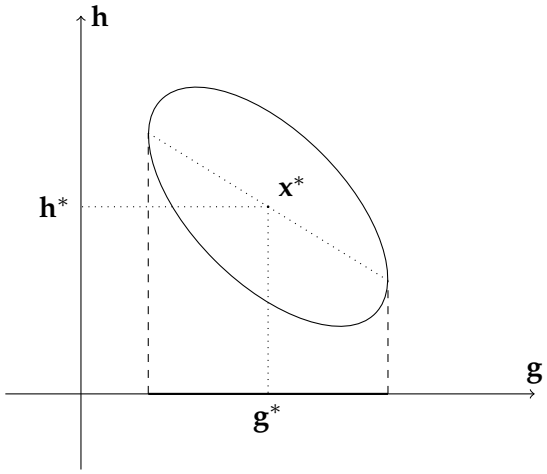

Figure 1.2.: Marginal ellipsoid of $\mathbf{g}$ for any value of $\mathbf{h}$.

which implies $\Gamma^{\mathbf{gg}} > \Gamma_{\mathbf{gg}}$. Thus, the marginal confidence ellipsoid contains the conditional confidence ellipsoid for $\mathbf{h} = \mathbf{h}^*$, that is the uncertainty of the $\mathbf{g}$ parameters is greater in this case.

- If $\mathbf{g} = x_1$, then $(C^{x_1x_1})^{-1} = \Gamma_{x_1x_1} = \gamma_{11}$ and the uncertainty is given by $\sqrt{\gamma_{11}}$, if $\sigma = 1$. This value is different from $1/\sqrt{c_{11}}$, as it is bigger.

1.3.3 *Conditional confidence ellipsoid for non-nominal values*

Fixing $\mathbf{h}$ to the non-nominal value $\mathbf{h}_0 \neq \mathbf{h}^*$, the expansion (1.3) becomes

$$\begin{aligned} m\Delta Q(\mathbf{x}) \simeq &(\mathbf{g}-\mathbf{g}^*)^T C_{\mathbf{gg}}(\mathbf{g}-\mathbf{g}^*) \\ &+ 2(\mathbf{g}-\mathbf{g}^*)^T C_{\mathbf{gh}}(\mathbf{h}_0-\mathbf{h}^*) + (\mathbf{h}_0-\mathbf{h}^*)^T C_{\mathbf{hh}}(\mathbf{h}_0-\mathbf{h}^*). \end{aligned}$$

The center $\mathbf{g}_0$ of the *conditional confidence ellipsoid* (see figure 1.3) is the minimum value of ΔQ when $\mathbf{h} = \mathbf{h}_0$, that is it is the solution of

$$m\frac{\partial \Delta Q}{\partial \mathbf{g}} = 0.$$

By omitting some computations, which can be found in [5], we conclude that the penalty ΔQ as function of $\mathbf{g} - \mathbf{g}_0$ has the following expression:

$$m\Delta Q = (\mathbf{g}-\mathbf{g}_0)^T C_{\mathbf{gg}}(\mathbf{g}-\mathbf{g}_0) + (\mathbf{h}_0-\mathbf{h}^*)^T C^{\mathbf{hh}}(\mathbf{h}_0-\mathbf{h}^*).$$

It means that the constraint $\mathbf{h} = \mathbf{h}_0$ implies a penalty $(\mathbf{h}_0-\mathbf{h}^*)^T C^{\mathbf{hh}}(\mathbf{h}_0-\mathbf{h}^*)$, which is a quadratic form of the difference $\mathbf{h}_0 - \mathbf{h}^*$, with matrix $C^{\mathbf{hh}} = \Gamma_{\mathbf{hh}}^{-1}$. It follows that

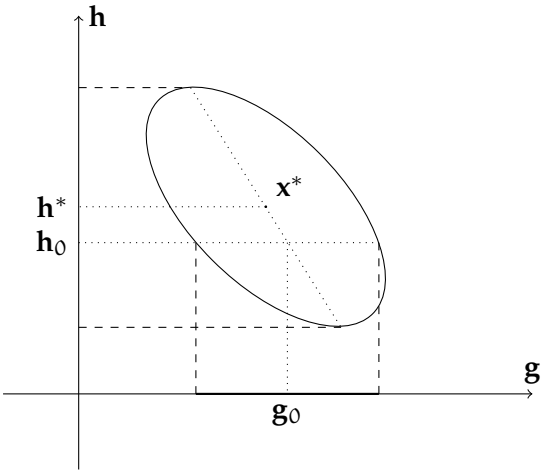

Figure 1.3.: Conditional confidence ellipsoid of $\mathbf{g}$ for $\mathbf{h} = \mathbf{h}_0$.

the conditional confidence ellipsoid in the $\mathbf{g}$ space is smaller than in the $\mathbf{h} = \mathbf{h}^*$ case, because

$$m\Delta Q \simeq \sigma^2 \Leftrightarrow (\mathbf{g} - \mathbf{g}_0)^T C_{\mathbf{gg}} (\mathbf{g} - \mathbf{g}_0) = \sigma^2 - (\mathbf{h}_0 - \mathbf{h}^*)^T C^{\mathbf{hh}} (\mathbf{h}_0 - \mathbf{h}^*)$$

and the last term is positive if $C^{\mathbf{hh}}$ is positive definite, which is the case when C and Γ are positive definite.

1.4 RANK DEFICIENCIES

The problem of orbit determination can't be separated from its numerical resolution. Indeed, if the normal matrix C is invertible, i.e. when the design matrix B is full rank, the normal equation has one solution that can be computed[1].
If C is not invertible, which is the case when B is rank deficient, the nominal solution is not well defined, therefore some "tricks" must be used. In this chapter we try to give a mathematical formulation of rank deficiency and propose some techniques to solve it (or avoid it).

1.4.1 *Exact rank deficiency and simmetries*

DEFINITION 1.20 - We say that a problem of orbit determination has a *rank deficiency of order* d if $\operatorname{rank} C = N - d$.

1 With some caution for the conditioning number of C.

REMARK 1.21 - If $\operatorname{rank} C = N - d$, then $\operatorname{rank} B = N - d$. This means that there exists a d-dimensioned linear subspace $V \subseteq \mathbb{R}^N$ such that

$$B\mathbf{v} = \mathbf{0} \quad \text{for all } \mathbf{v} \in V.$$

Thus, for all $s \in \mathbb{R}$, $\mathbf{v} \in V$, $\mathbf{x} \in \mathbb{R}^N$ we have

$$\begin{aligned} \xi(\mathbf{x} + s\mathbf{v}) &= \xi(\mathbf{x}) + s\frac{\partial \xi}{\partial \mathbf{x}}(\mathbf{x})\mathbf{v} + o(s^2) \\ &= \xi(\mathbf{x}) + o(s^2). \end{aligned}$$

The previous relation says that some linear combinations of the parameters are uninfluential on the residuals, therefore they can't be constrained by the least squares optimization.

A way to individuate rank deficiencies is to look for symmetries in the problem of orbit determination.

DEFINITION 1.22 - Let G be a group of transformations of $\mathbb{R}^N$. We say that G is a *group of exact symmetries* if

$$\xi(g[\mathbf{x}]) = \xi(\mathbf{x}) \quad \text{for all } g \in G.$$

The following theorem shows what we were saying before. A proof can be found in [5].

THEOREM 1.23 - *If* G *is a one-parameter group of exact symmetries of an orbit determination problem and the following condition of non-isotropy holds,*

$$g[\mathbf{x}] = \mathbf{x} \text{ for all } \mathbf{x} \in \mathbb{R}^N \Longrightarrow g = \mathrm{id},$$

then there exists an exact rank deficiency of order $d \geqslant 1$.

Under stricter hypothesis, it can be shown that the converse is true, too. In substance we may conclude that rank deficencies and exact symmetries are correlated and looking for one is equivalent to looking for the other.

1.4.2 *Some remedies to rank deficiency*

In this section we describe two ways to solve rank deficiency.

DESCOPING It consists in selecting d parameters from the list of the fit parameters and moving them into the consider parameters, assigning them some nominal value, which can come from previous observations or be arbitrary. This way, the design matrix becomes full rank.

A PRIORI OBSERVATIONS We assume to have some more information on all or some of the parameters $\mathbf{x}$ and we add it to the observations with suitable weights. If $\mathbf{x}_P := (x_i^P) \in \mathbb{R}^N$ is a set of assumed values for $x_1, \dots, x_N$, each with weight $1/\sigma_i$, we can define $C_P := \mathrm{diag}(\sigma_1^{-2}, \dots, \sigma_N^{-2})$ and write the a priori normal equation

$$C_P \mathbf{x} = C_P \mathbf{x}_P.$$

This equation corresponds to an a priori target function

$$Q_P := \frac{1}{(m+N)} (\mathbf{x} - \mathbf{x}_P)^T C_P (\mathbf{x} - \mathbf{x}_P),$$

which we add to the original one:

$$Q_{tot} := \frac{m}{m+N} Q + \frac{N}{m+N} Q_P.$$

The complete normal equation, obtained neglecting higher order terms, is

$$[C_P + B^T B](\mathbf{x}_{k+1} - \mathbf{x}_k) = -B^T \boldsymbol{\xi} + C_P(\mathbf{x}_P - \mathbf{x}_k).$$

REMARK 1.24 - The values σ_i^2 represent the variances of the a priori observations. If they are small enough, $C := B^T B + C_P$ is full rank and the rank deficiency is cured. A priori values of dynamical and kinetical parameters can come from results obtained from previous missions, while a priori values on $\mathbf{y}_0$ correspond to know in advance some characteristics of the orbit.

1.4.3 *Approximate rank deficiency and symmetries*

Exact rank deficiency is not the only source of numerical instability. We must consider the case when the normal matrix is full rank, but it has some small eigenvalues.

DEFINITION 1.25 - An *approximate rank deficiency* of order $d \geqslant 1$ is the existence of a linear subspace $V \subseteq \mathbb{R}^N$ of dimension d, not $d+1$, and of $0 < \epsilon \ll 1$ such that for all $\mathbf{v} \in V, |\mathbf{v}| = 1$, it holds $|B\mathbf{v}| \leqslant \epsilon$.

THEOREM 1.26 - *Let $0 \leqslant \lambda_1 \leqslant \cdots \leqslant \lambda_N$ the eigenvalues of the normal matrix C. If there is an approximate rank deficiency of order d, then $\lambda_1, \dots, \lambda_d \leqslant \epsilon^2$.*

REMARK 1.27 - In presence of an approximate rank deficiency of order d, the confidence ellipsoid $Z_L(1)$ has d semiaxis longer than $1/\epsilon$. The converse is also true: if there are d semiaxis longer than $1/\epsilon$, then the subspace spanned by those vectors satisfies the definition of approximate rank deficiency of order d.

As in the case of exact rank deficiency, the presence of an approximate rank deficiency corresponds to the existence of an approximate symmetry. To define it, we look at the definition of exact symmetry and combine it with the idea of approximation.

DEFINITION 1.28 - Let G be a group of transformations of $\mathbb{R}^N$. We say that G is a *group of approximate symmetries* if

$$\xi(g[\mathbf{x}]) = \xi(\mathbf{x}) + \epsilon\mathbf{a} + O(\epsilon^2), \quad \mathbf{a} \in \mathbb{R}^m, \ |\mathbf{a}| = 1, \ \text{ for all } g \in G.$$

The following theorem is the analogous of (1.23).

THEOREM 1.29 - *If* G *is a one-parameter group of approximate symmetries of an orbit determination problem and the condition of isotropy holds, then there exists an approximate rank deficiency of order* $d \geqslant 1$.

Therefore, when we want some information on degenaricity of the normal matrix, we can look for approximate symmetries.

2

THE GRAVITY FIELD OF A PLANET

In this chapter we deal with the problem of giving a mathematical representation of the gravity field of a planet: we introduce the gravitational potential, show its properties and describe the spherical harmonics expansion. Then, we treat the Kaula expansion, which gives a representation of the gravitational potential in terms of the keplerian elements of an orbit around the planet. For further details, see [3] or [5].

2.1 THE GRAVITATIONAL POTENTIAL

First we must specify what we mean by planet.

DEFINITION 2.1 - An *extended body* is a limited set $W \subset \mathbb{R}^3$ with a *mass density function* $\rho\colon \mathbb{R}^3 \to \mathbb{R}$ everywhere non-negative, positive only on W. The *mass* of the extended body is

$$M := \int_W \rho(\mathbf{p}) d\mathbf{p}.$$

When we deal with a planet, we indicate with $R_\oplus$ the radius of a sphere strictly containing the planet. We can think of $R_\oplus$ as the equatorial radius of the planet.
Now we can define the gravity field and the gravitational potential generated by a mass distribution, by means of some integral formulæ.

DEFINITION 2.2 - The *gravity field* generated by the mass density ρ is

$$\mathbf{v}(\mathbf{x}) := \int_W \frac{G\rho(\mathbf{p})}{|\mathbf{x}-\mathbf{p}|^3}(\mathbf{p}-\mathbf{x}) d\mathbf{p}.$$

The *gravitational potential* of the extended body W is

$$U(\mathbf{x}) := \int_W \frac{G\rho(\mathbf{p})}{|\mathbf{x}-\mathbf{p}|} d\mathbf{p}. \tag{2.1}$$

REMARK 2.3 - Note that $\operatorname{grad} U(\mathbf{x}) = \mathbf{v}(\mathbf{x})$; by the *divergence formula*, it can be shown that

$$\operatorname{div} \mathbf{v}(\mathbf{x}) = -4\pi G\rho(\mathbf{x}),$$

hence we conclude that

$$\Delta U(\mathbf{x}) = \begin{cases} 0 & \mathbf{x} \notin W \\ -4\pi G\rho(\mathbf{x}) & \mathbf{x} \in W. \end{cases}$$

We recall that a function f satisfying the *Laplace equation* $\Delta f = 0$ is harmonic. Thus, the gravitational potential U is a harmonic function in $\mathbb{R}^3 \setminus W$, therefore analytic in the same domain. It follows that solutions of equations of motion

$$\frac{d^2\mathbf{x}}{dt^2} = \mathbf{v}(\mathbf{x}),$$

where they exist and in every non singular point, are analytic, too.

2.2 SPHERICAL HARMONICS

From now on, we consider planets with nearly spherical shape and use spherical coordinates in place of cartesian coordinates:

$$\begin{cases} x := r\cos\theta\cos\lambda \\ y := r\cos\theta\sin\lambda \\ z := r\sin\theta, \end{cases} \tag{2.2}$$

where $r > 0$ is the *distance from the center*, $\theta \in [-\pi/2, \pi/2]$ is the *latitude*, $\lambda \in [0, 2\pi]$ is the *longitude*.

EXAMPLE 2.4 - On the Earth, a reference frame in which x, y axis span the equatorial plane and z is the rotation axis is often used.

The gravitational potential of a planet can be expressed in spherical coordinates: $U(x, y, z) = \Phi(r, \theta, \lambda)$. We are interested in a representation of the potential outside the planet, therefore we look for solutions of the Laplace equation. To do this, we need the expression of the Laplace operator in spherical coordinates:

$$r^2\Delta\Phi = \frac{\partial}{\partial r}\left(r^2\frac{\partial\Phi}{\partial r}\right) + \Delta_S\Phi,$$

where

$$\Delta_S\Phi = \frac{1}{\cos\theta}\frac{\partial}{\partial\theta}\left(\cos\theta\frac{\partial\Phi}{\partial\theta}\right) + \frac{1}{\cos^2\theta}\frac{\partial^2\Phi}{\partial\lambda^2}$$

is the *Laplace-Beltrami* operator.

2.2.1 *Zonal harmonics*

Before we deal with the general case, we search for solutions of the Laplace equation which are independent of the longitude λ; this is the case of an axial symmetric planet. Thus $U(x, y, z) = \Phi(r, \theta)$ and Laplace equation is

$$\Delta\Phi = \frac{1}{r^2}\frac{\partial}{\partial r}\left[r^2\frac{\partial\Phi}{\partial r}\right] + \frac{1}{r^2\cos\theta}\frac{\partial}{\partial\theta}\left[\cos\theta\frac{\partial\Phi}{\partial\theta}\right] = 0. \tag{2.3}$$

We solve the preceeding equation by *separation of variables*, that is by searching for solutions of the form

$$\Phi(r, \theta) = R(r)F(\theta).$$

We omitt the detailed solution, which can be found in [5], and limit ourselves in concluding that there exist two linearly independent solutions of equation (2.3) for each integer $\ell \geqslant 0$, the *zonal spherical harmonics*

$$P_\ell(\sin\theta)\frac{1}{r^{\ell+1}}, \qquad P_\ell(\sin\theta)r^\ell,$$

where P_ℓ is the *Legendre polynomial of degree* ℓ,

$$P_\ell(x) = \frac{1}{2^\ell \ell!}\frac{d^\ell}{dx^\ell}(x^2-1)^\ell.$$

The first solutions are the *external harmonics*, which describe the gravity field outside an extended body, and the second ones are the *internal harmonics*, which describe the gravitational potential inside a cavity surrounded by a mass distribution. We consider only the external harmonics, as they are the only ones of interest for our aims.

2.2.2 *Tesseral harmonics*

In the most general case we don't have any symmetry of the potential, therefore searching for solutions by separation of variables leads us to functions of the form $U = \Phi(r, \theta, \lambda) = R(r)F(\theta)G(\lambda)$. Again, we don't give a complete description of the solution, but we straightly conclude that four linearly independent solutions can be found for every (ℓ, m):

- the *external tesseral spherical harmonics*,

$$\frac{P_{\ell m}(\sin\theta)}{r^{\ell+1}}\cos(m\lambda), \qquad \frac{P_{\ell m}(\sin\theta)}{r^{\ell+1}}\sin(m\lambda),$$

  where $P_{\ell m}$ is the *Legendre associated function of degree* ℓ *and order* m (see [5] for an analytic expression);

- the *internal* tesseral spherical harmonics, which are the counterpart of the internal zonal harmonics, and again we won't consider them.

REMARK 2.5 - For $m = 0$ we obtain the zonal spherical harmonics, previously described.

2.2.3 *Expansion in spherical harmonics*

By linearity of the Laplace operator, we have that any linear combination of spherical harmonics is still solution of the Laplace equation; we write the generic solution as follows:

$$U = \frac{GM}{r}\left\{\sum_{\ell=0}^{\infty}\sum_{m=0}^{\ell} P_{\ell m}(\sin\theta)\frac{R_\oplus^\ell}{r^\ell}[C_{\ell m}\cos(m\lambda) + S_{\ell m}\sin(m\lambda)]\right\}, \tag{2.4}$$

where we have added the equatorial radius $R_\oplus$ of the planet to have adimensional *harmonic coefficients* $(C_{\ell m})_{0\leqslant m\leqslant l}$ $(S_{\ell m})_{0<m\leqslant \ell}$ and we define by convention $P_{\ell 0} := P_\ell$, $P_0 := 1$.

Let's see some properties of the harmonic coefficients.

Remarks 2.6 • Let $\mathbf{c}$ be the coordinates of the center of mass of the planet. It can be shown that

$$(C_{11}, S_{11}, C_{10}) = \mathbf{c}/R_\oplus.$$

Thus, in a suitable frame centered at the center of mass, the harmonic coefficients of degree 1 are zero.

- Let (I_{ij}), $i,j = 1,2,3$ be the *moments of inertia* of the planet. Then, the following relations hold:

$$C_{20} = \frac{1}{MR_\oplus^2}\left[\frac{I_{11}+I_{22}}{2} - I_{33}\right], \quad C_{22} = \frac{1}{4MR_\oplus^2}(I_{22}-I_{11})$$
$$C_{21} = -\frac{1}{MR_\oplus^2}I_{13}, \quad S_{21} = -\frac{1}{MR_\oplus^2}I_{23}, \quad S_{22} = -\frac{1}{2MR_\oplus^2}I_{12}.$$

2.3 PROPERTIES OF SPHERICAL HARMONICS

In this section we show very useful properties of spherical harmonics, which are of interest for the representation of the gravitational potential of any given planet. We prove that the set of spherical harmonics on the sphere S^2 is an orthonormal basis for $L^2(S^2)$, stating the possibility to expand any reasonable function on the sphere in spherical harmonics series. Secondly, we show the convergence of the expansion (2.4) in $\mathbb{R}^3$ except an open ball containing the extended body W, which ensures that the spherical harmonics series is a good representation for the gravitational potential of a planet.

2.3.1 *Orthonormality*

First of all, let's rewrite (2.4) in a different way: by defining

$$Y_{\ell m i}(\theta,\lambda) := \begin{cases} P_{\ell m}(\sin\theta)\cos(m\lambda) & i = 1 \\ P_{\ell m}(\sin\theta)\sin(m\lambda) & i = 0 \\ 0 & m = 0,\ i = 0, \end{cases}$$

which are spherical harmonics on the unit sphere, we have that

$$U = \frac{GM}{r}\sum_{\ell=0}^{\infty}\frac{R_{\oplus}^{\ell}}{r^{\ell}}\sum_{m=0}^{\ell}[C_{\ell m}Y_{\ell m1} + S_{\ell m}Y_{\ell m0}]. \tag{2.5}$$

On the set of the functions on the unit sphere S^2 we define the L^2 *scalar product*:

$$\langle f, g\rangle_2 := \int_{S^2} fg\, dS. \tag{2.6}$$

Before we prove the main result of this section, we need a lemma.

LEMMA 2.7 - *The Laplace-Beltrami operator is self-adjoint with respect to the* L^2 *scalar product, that is*

$$\langle \Delta_S f, g\rangle_2 = \langle f, \Delta_S g\rangle_2 \quad \textit{for all} \quad f, g.$$

Proof. The result follows from an integration by parts: recalling that the element of surface of the sphere S^2 is $dS = \cos\theta d\theta d\lambda$,

$$\begin{aligned}
\langle \Delta_S f, g\rangle_2 &= \int_{S^2} \Delta_S f\ g dS \\
&= \int_0^{2\pi}\int_{-\frac{\pi}{2}}^{\frac{\pi}{2}}\left[\frac{1}{\cos\theta}\frac{\partial}{\partial\theta}\left(\cos\theta\frac{\partial f}{\partial\theta}\right) + \frac{1}{\cos^2\theta}\frac{\partial^2 f}{\partial\lambda^2}\right] g\cos\theta d\theta d\lambda \\
&= \int_0^{2\pi} d\lambda\int_{-\frac{\pi}{2}}^{\frac{\pi}{2}}\frac{\partial}{\partial\theta}\left(\cos\theta\frac{\partial f}{\partial\theta}\right) g d\theta + \int_{-\frac{\pi}{2}}^{\frac{\pi}{2}}\frac{1}{\cos\theta}d\theta\int_0^{2\pi}\frac{\partial^2 f}{\partial\lambda^2}g d\lambda \\
&= \int_0^{2\pi} d\lambda\left[\cos\theta\frac{\partial f}{\partial\theta}g\Big|_{-\frac{\pi}{2}}^{\frac{\pi}{2}} - \int_{-\frac{\pi}{2}}^{\frac{\pi}{2}}\cos\theta\frac{\partial f}{\partial\theta}\frac{\partial g}{\partial\theta}d\theta\right] \\
&+ \int_{-\frac{\pi}{2}}^{\frac{\pi}{2}}\frac{1}{\cos\theta}d\theta\left[\frac{\partial f}{\partial\lambda}g\Big|_0^{2\pi} - \int_0^{2\pi}\frac{\partial f}{\partial\lambda}\frac{\partial g}{\partial\lambda}d\lambda\right] \\
&= -\int_0^{2\pi} d\lambda\int_{-\frac{\pi}{2}}^{\frac{\pi}{2}}\cos\theta\frac{\partial f}{\partial\theta}\frac{\partial g}{\partial\theta}d\theta - \int_{-\frac{\pi}{2}}^{\frac{\pi}{2}}\frac{1}{\cos\theta}d\theta\int_0^{2\pi}\frac{\partial f}{\partial\lambda}\frac{\partial g}{\partial\lambda}d\lambda,
\end{aligned} \tag{2.7}$$

the last passage holding because $\cos(\pi/2) = \cos(-\pi/2) = 0$ and continuous functions on the sphere have the same values on $\lambda = 0, 2\pi$. Since (2.7) is symmetric with respect to the interchange of f and g, the lemma is proved. □

The following theorem holds.

THEOREM 2.8 - *The set of spherical harmonics* $(Y_{\ell mi})$ *is orthogonal with respect to the* L^2 *scalar product.*

Proof. We have to prove that

$$\langle Y_{\ell mi}, Y_{\ell' m' i'} \rangle_2 = 0 \quad \text{if } (\ell, m, i) \neq (\ell', m', i').$$

To do this, we use that $(Y_{\ell mi})$ are eigenfunctions of the Laplace-Beltrami operator, i.e.

$$\Delta_S Y_{\ell mi} = -\ell(\ell+1) Y_{\ell mi},$$

which comes from an easy computation. Thus, using Lemma 2.7,

$$\begin{aligned} -\ell(\ell+1)\langle Y_{\ell mi}, Y_{\ell' m' i'} \rangle_2 &= \langle \Delta_S Y_{\ell mi}, Y_{\ell' m' i'} \rangle_2 \\ &= \langle Y_{\ell mi}, \Delta_S Y_{\ell' m' i'} \rangle_2 \\ &= -\ell'(\ell'+1)\langle Y_{\ell mi}, Y_{\ell' m' i'} \rangle_2, \end{aligned}$$

from which it's clear that if $\ell \neq \ell'$, then $\langle Y_{\ell mi}, Y_{\ell' m' i'} \rangle = 0$.

For the other cases, we write the integral expression of the scalar product

$$\begin{aligned} \langle Y_{\ell mi}, Y_{\ell' m' i'} \rangle &= \int_{S^2} P_{\ell m} P_{\ell' m'} \operatorname{trig}(m\lambda, i) \operatorname{trig}(m'\lambda, i') \, dS \\ &= \int_0^{2\pi} \operatorname{trig}(m\lambda, i) \operatorname{trig}(m'\lambda, i') d\lambda \int_{-\frac{\pi}{2}}^{\frac{\pi}{2}} P_{\ell m} P_{\ell' m'} \cos\theta \, d\theta, \end{aligned} \tag{2.8}$$

where

$$\operatorname{trig}(x, i) := \begin{cases} \sin x & i = 0 \\ \cos x & i = 1. \end{cases}$$

It comes from the property of orthogonality of trigonometric functions that (2.8) is zero if $m \neq m'$ or $i \neq i'$. □

The set of the spherical harmonics on the sphere $(Y_{\ell mi})$ is not orthonormal. We can normalize them using the scalar product $\langle f, g \rangle := (4\pi)^{-1} \langle f, g \rangle_2$, as proposed in [3]: this way, the *normalized spherical harmonics* are defined by

$$\overline{Y}_{\ell mi} = \frac{Y_{\ell mi}}{\sqrt{\langle Y_{\ell mi}, Y_{\ell mi} \rangle}} = \sqrt{\frac{(2-\delta_{0m})(2\ell+1)(\ell-m)!}{(\ell+m)!}} \, Y_{\ell mi} =: H_{\ell m} Y_{\ell mi},$$

and have unit quadratic mean on the sphere ($\delta_{0m} = 1$ if $m = 0$ and zero otherwise). We can rewrite (2.5) by using the new functions:

$$U = \frac{GM}{r} \sum_{\ell=0}^{\infty} \frac{R_\oplus^\ell}{r^\ell} \sum_{m=0}^{\ell} [\overline{C}_{\ell m} \overline{Y}_{\ell m 1} + \overline{S}_{\ell m} \overline{Y}_{\ell m 0}], \tag{2.9}$$

where $\overline{C}_{\ell m} = C_{\ell m}/H_{\ell m}$ and $\overline{S}_{\ell m} = S_{\ell m}/H_{\ell m}$ are the *normalized harmonic coefficients*.

2.3.2 *Convergence*

We would like to know whether the spherical harmonics series is a good representation of the potential, that is if it converges and in which cases.

THEOREM 2.9 - *If the support W of the mass distribution ρ is contained in the open ball $\{|\mathbf{x}| < R_\oplus\}$, then the expansion in spherical harmonics (2.4) is uniformly convergent for $|\mathbf{x}| > R_\oplus$.*

Proof. We only give an idea of the proof. It is known that the complex variable function $f(z) := (1+z)^{-\frac{1}{2}}$ is holomorphic if $|z| < 1$; it follows that the spherical harmonics expansion of the function

$$\frac{1}{|\mathbf{x}-\mathbf{p}|} = \sum_{\ell=0}^{\infty} \frac{|\mathbf{p}|^\ell}{|\mathbf{x}|^{\ell+1}} P_\ell(\cos\theta)$$

is uniformly convergent on each sphere $\{|\mathbf{x}| = r\}$ with $r > |p|$. From (2.1), by continuity of the integral operator, we conclude that the spherical harmonics expansion is convergent if $|\mathbf{x}| > R_\oplus$. □

REMARK 2.10 - We would like to know whether the series (2.4) is convergent even for $|\mathbf{x}| = R_\oplus$. In this case we use an argument from [3] to show the convergence. From a descriptive statistics of data concerning the Earth gravity field, the following formula is obtained:

$$\mathrm{RMS}(\overline{C}_{\ell m}) = \mathrm{RMS}(\overline{S}_{\ell m}) = \frac{K}{\ell^2}.$$

By computing the L^2 norm of the expansion, we have

$$\|U\|_2 \simeq \sum_\ell \frac{K}{\ell^2}\,\frac{K}{\ell^2}\,(2\ell+1) \simeq \sum_\ell \frac{c}{\ell^3} < +\infty,$$

therefore the series is convergent in the L^2 norm for $|\mathbf{x}| = R_\oplus$.
If the sum of the series is a function $f \in \mathscr{C}^1(S^2)$, then the series is also uniformly convergent (see [1]). It is in general not true if $f \in \mathscr{C}(S^2)$.

2.3.3 *Completeness*

Another important property of the spherical harmonics set $(\overline{Y}_{\ell mi})$ is completeness.

THEOREM 2.11 - *The set $(\overline{Y}_{\ell mi})$ is an orthonormal complete set in the Hilbert space $L^2(S^2)$.*

Proof. The proof is divided in two steps.

First, we show that $(\overline{Y}_{\ell mi})$ is dense in $\mathscr{C}(S^2)$ with respect to the L^∞ norm. For any given $g \in \mathscr{C}(S^2)$, by Stone-Weierstrass theorem, for all $\epsilon > 0$ we can find a polynomial

p on S^2 such that $\|g - p\|_\infty < \epsilon$. Now, every polynomial on the sphere S^2 is sum of spherical harmonics (see [9], pag. 140, Corollary 2.2), and the first part is proved.

Let now be $f \in L^2(S^2)$; it is known that for all $\epsilon > 0$ there exists a continuous function g such that $\|f - g\|_2 < \epsilon/2$. Let h be a linear combination of spherical harmonics as in the previous step:

$$\|g - h\|_\infty < \frac{\epsilon}{2\sqrt{\mathrm{vol}(S^2)}}.$$

Therefore,

$$\begin{aligned}\|f - h\|_2 &\leqslant \|f - g\|_2 + \|g - h\|_2 \\ &< \frac{\epsilon}{2} + \|g - h\|_\infty \sqrt{\mathrm{vol}(S^2)} < \epsilon,\end{aligned}$$

which completes the proof. □

2.3.4 *Exterior Dirichlet problem*

An important consequence of the latter theorems is the solution to the *exterior Dirichlet problem*, that is finding a function $\Phi(r, \theta, \lambda)$, defined on the complementary of a ball of radius $R_\oplus$, such that

$$\begin{cases} \Delta\Phi = 0 & \text{if } r > R_\oplus \\ \Phi(R_\oplus, \theta, \lambda) = f(\theta, \lambda) & \text{if } r = R_\oplus, \end{cases}$$

where $f \in \mathscr{C}(S^2)$. Indeed, theorem 2.11 ensures we can expand $f(\theta, \lambda)$ in series of spherical harmonics and theorem 2.8 tells that its harmonic coefficients can be computed using

$$\begin{aligned}\overline{C}_{\ell m} &= \langle f, \overline{Y}_{\ell m 1}\rangle_2 \cdot \frac{1}{4\pi}\frac{R_\oplus}{GM}, \\ \overline{S}_{\ell m} &= \langle f, \overline{Y}_{\ell m 0}\rangle_2 \cdot \frac{1}{4\pi}\frac{R_\oplus}{GM}, \\ \overline{C}_{\ell 0} &= \langle f, \overline{Y}_{\ell 0 1}\rangle_2 \cdot \frac{1}{4\pi}\frac{R_\oplus}{GM}.\end{aligned}$$

Thus, we can define Φ by the uniformly convergent series (theorem 2.9)

$$\Phi = \frac{GM}{r}\sum_{\ell=0}^{\infty}\frac{R_\oplus^\ell}{r^\ell}\sum_{m=0}^{\ell}[\overline{C}_{\ell m}\overline{Y}_{\ell m 1} + \overline{S}_{\ell m}\overline{Y}_{\ell m 0}],$$

which is obviously equal to f if $r = R_\oplus$. Moreover, Φ is uniquely defined because if there were two such functions, say Φ_1, Φ_2, their difference $\widehat{\Phi}$ would solve the exterior Dirichlet problem

$$\begin{cases} \Delta\widehat{\Phi} = 0 & \text{if } r > R_\oplus \\ \widehat{\Phi} = 0 & \text{if } r = R_\oplus, \end{cases}$$

thus $\widehat{\Phi}$ would be zero, which implies $\Phi_1 = \Phi_2$.

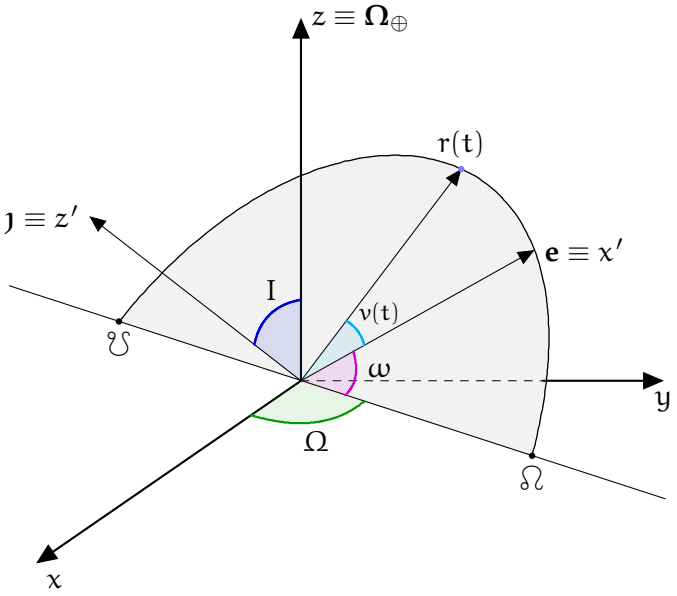

Figure 2.1.: The xyz frame and the $x'y'z'$ frame. The planet is pointwise for simplicity of representation.

2.4 KAULA EXPANSION

When a satellite is in orbit around a planet W, the gravitational potential at each point $\mathbf{x}$ of the orbit has the expression (2.4). We would like to have a similar formula which expresses the gravity field along the orbit in terms of the keplerian elements $e, a, I, \omega, \Omega, l$ of the orbit (see appendix A.1), in the hypothesis of two body motion. We write the gravitational potential as

$$U = \frac{GM}{r} + \sum_{\ell=2}^{\infty} \sum_{m=0}^{\ell} U_{\ell m}, \tag{2.10}$$

where the sum starts from degree 2 thanks to remark (2.6).

THEOREM 2.12 - *The gravitational potential* U *of a planet as function of the keplerian elements of the orbit of a satellite has expression (2.10), where*

$$U_{\ell m} = \frac{GMR_{\oplus}^{\ell}}{a^{\ell+1}} \sum_{p=0}^{\ell} F_{\ell m p}(I) \sum_{q=-\infty}^{+\infty} G_{\ell p q}(e)[C_{\ell m} \cos(\psi_{\ell m p q}) + S_{\ell m} \sin(\psi_{\ell m p q})]$$

and

$$\psi_{\ell m p q} = (\ell - 2p)\omega + (\ell - 2p + q)l + m(\Omega - \phi) - \frac{\pi}{2}[(\ell - m) \bmod 2].$$

REMARK 2.13 - The functions $F_{\ell mp}(I)$, $G_{\ell pq}(e)$ are respectively called *inclination functions* and *eccentricity functions*, and their (quite complicated) expressions can be found in [3] up to $\ell pq = 442$.

Let xyz be the axis of the frame in which xy span the equatorial plane of the planet and z is the rotation axis and let $x'y'z'$ be the axis of the frame in which $x'y'$ span the orbit plane, x' is the direction of the pericenter and z' is parallel to the angular momentum $\mathfrak{J}$ (see figure 2.1). The proof of the previous theorem bases on a linear change of coordinates from the xyz frame to the $x'y'z'$. The matrix giving the change of coordinates is a composition of three rotation matrices, respectively of angles $\omega, \Omega - \phi$, where ϕ is the phase of rotation of the planet, and I.

EXAMPLE 2.14 - If $I = 0°$, that is for *equatorial orbits*, Kaula expansion assumes a simpler form. In this case the keplerian element Ω is not defined: we use ϖ, the angle between the x axis and the direction of the pericenter; note that in this case $\phi = \Omega_\oplus(t - t_0)$, therefore $U_{\ell m}$ has the form

$$U_{\ell m} = \frac{GMR_\oplus^\ell}{r^{\ell+1}} P_{\ell m}(0)[C_{\ell m}\cos(\psi_m) + S_{\ell m}\sin(\psi_m)],$$

where

$$\psi_m = m\lambda = m[\nu + \varpi - \Omega_\oplus(t - t_0)].$$

For the special case of circular orbit, we have $e = 0$ and ϖ is no more defined. In this case the true anomaly ν is equal to the mean anomaly l, therefore

$$\psi_m = m(n - \Omega_\oplus)(t - t_0).$$

It follows that harmonics with the same order share the same frequencies. Informally speaking, a satellite orbiting a planet with an equatorial circular orbit cannot distinguish between coefficients $C_{\ell m}$ and $C_{\ell' m}$, for instance. As the same happens for the sine coefficients $S_{\ell m}$, the probe "sees" only 2 frequencies per harmonic degree ℓ. It follows that the orbit determination problem of recovering the harmonic coefficients of the gravitational potential of a planet has an exact rank deficiency of order $(\ell_{max} + 1)^2 - 4 - 2(\ell_{max} - 1)$, where ℓ_{max} is the maximum degree in the truncation of the potential expansion.
In conclusion, circular equatorial orbits are not indicated for the determination of the gravity field of a planet: near polar orbits ($\simeq I = 90°$) are preferable.

3 THE JUNO MISSION

In this chapter we describe NASA's Juno mission to Jupiter, a project which is part of NASA *New Frontiers* Program, a series of space missions aiming to study the most important celestial bodies of the Solar System. The main reference, where all the figures have been taken from, is [4].

3.1 MISSION GOALS

Juno mission was designed to reveal the story of formation and evolution of planet Jupiter. This will also improve the current knowledge of the Solar System's beginnings, as it will make clear which role had Jupiter in the formation of our planetary system. This will help understand planetary systems around other stars.
Juno's scientific objectives can be summarized in four points:

ORIGIN Juno will determine the Oxygen/Hydrogen ratio and Nitrogen concentration, in order to discriminate among Jupiter formation scenarios;

INTERIOR Juno will reveal Jupiter's interior structure and the movement of its internal materials by mapping its gravitational and magnetic fields;

ATMOSPHERE Variations in atmospheric composition, temperature, cloud opacity and dynamics will be mapped by sounding to pressures greater than 100 bars using microwave frequencies;

MAGNETOSPHERE The three-dimensional structure of Jupiter's polar magnetosphere and aurorae will be explored.

The second scientific objective is the one which interests us the most, as it requires the *Gravity Science experiment* to be performed: mapping Jupiter's gravity field is important to explore the distribution of mass inside the planet. Indeed, the lowest zonal harmonics, C_2, C_4 and C_6 give constraints on the mass of the core: they show the non-linear centrifugal response of the planet to its own rotation, whose effect on these harmonics depends on the extent to which the planet's mass is concentrated towards the center. These coefficients are required to be known except for an uncertainty of $\pm 10^{-7}$. Moreover, coefficients C_8 to C_{14} help determining the depth of zonal winds.

Juno will achieve the goals just described by means of a spinning, solar-powered spacecraft, which will be inserted in a unique polar orbit with a close perijove.

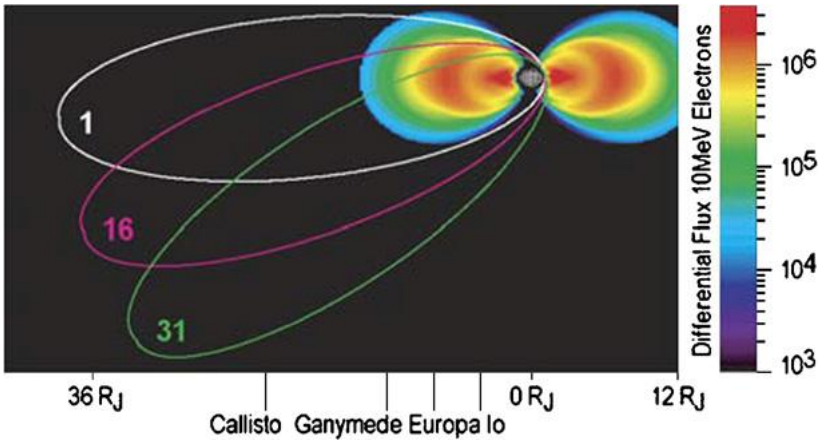

Figure 3.1.: The spacecraft's highly eccentric orbit will keep the probe away from Jupiter's radiation most of the mission. The figure also shows the line of apsides' precession.

3.2 MISSION DESIGN

Juno probe has been launched on August 5, 2011, and requires a 5-years cruise to reach Jupiter. Two years after the launch (October 2013) an Earth flyby will ensure additional energy to reach Jupiter. The spacecraft's arrival at Jupiter and its orbit insertion are foreseen on July, 2016.
The mission will last about one Earth-year, during when the probe will orbit Jupiter 32 times, each orbit requiring about 11 days to be completed. The orbit is polar (inclination $I = 90°$ over the planet's equator) and highly eccentric, with the perijove at about $1.06R_{\mathcal{U}}$, the apojove at about $39R_{\mathcal{U}}$. This will let Juno spend most of the mission away from Jupiter's radiation environment.
During the mission, the line of apsides of the orbit will preceed as a consequence of Jupiter's oblateness (see appendix A.2): the starting latitude of the pericenter is 6°N, getting up to 34°N in the last orbit (see figure 3.1).
The nominal mission ends with a deorbit into Jupiter's atmosphere in order to avoid planetary contamination from terrestrial microbes.

3.3 PAYLOAD

There are five main elements in the science instrument suite: a Microwave Radiometer (MWR), a Magnetometer, Gravity Science (GS), Fields and Particles instruments and The JunoCam. A full description of all of them goes beyond the scope of this work, so we focus our attention on GS, as it is the one straightly related to the topic we deal with.

Gravity Science

The Italian Space Agency (ASI) furnished the Ka-band (26.5 to 40 GHz) system the spacecraft has been equipped with. This investigation processes Ka-band telemetry on the ground via the telecom subsystem, augmented with a Ka-band Translator and Downconverter enabling a two way Ka radio science link with the Deep Space Network (DSN). X-band is also utilized with this investigation to yield X up/down and Ka up/down simultaneously. With this instrumentation, the Doppler tracking of the spacecraft can be performed with a precision of 3×10^{-4} cm/s: the signal being sent from Earth is caught by the spacecraft antenna, remodulated and then sent back to Earth.

3.4 SPACECRAFT

The Juno mission requires a spinning spacecraft to achieve its science objectives. This feature ensures stability and eliminates the need for attitude control components, which are complex and power-hungry. Moreover, the probe remains continuously in sunlight from launch through end of mission, except for a 10-minutes period during Earth Flyby. This results in stable thermal conditions and maximum solar array power production. The instruments are protected from Jovian radiative environment by a radiation-shielded electronics vault, which has never been used before in a space mission. However, the radiation is so destructive that the JunoCam is planned to work until orbit 8, while the MWR until orbit 11.

3.5 OPERATIONS

During the cruise, there will be many chances to do some training. For example:

- The Deep Space Maneuvre, which will direct the S/C towards the Earth, is a chance to rehearse the Jupiter Orbit Insertion;
- the Earth Flyby will be a chance to rehearse the perijove passage;
- every 12-18 months instruments calibrations are taken.

During each orbit, the closest approach will last 6 hours, during when science measurements will be taken. Outside of this perijove time, collected datas will be sent to Earth. Furthermore, orbit 2 and orbits 4 to 7 will be used for MWR measurements, while orbit 3 and orbits 8 to 32 are planned for Gravity Science experiments (see figure 3.2). When GS mode is on, the High Gain Antenna will point to the Earth. The equatorial crossings all occur at equal longitude spacing: for orbits 2-16 this spacing is 24°, and a maneuvre after perijove of orbit 16 will adjust the longitude crossing by 12°, ensuring an ultimate longitude spacing of 12° (see figure 3.3).

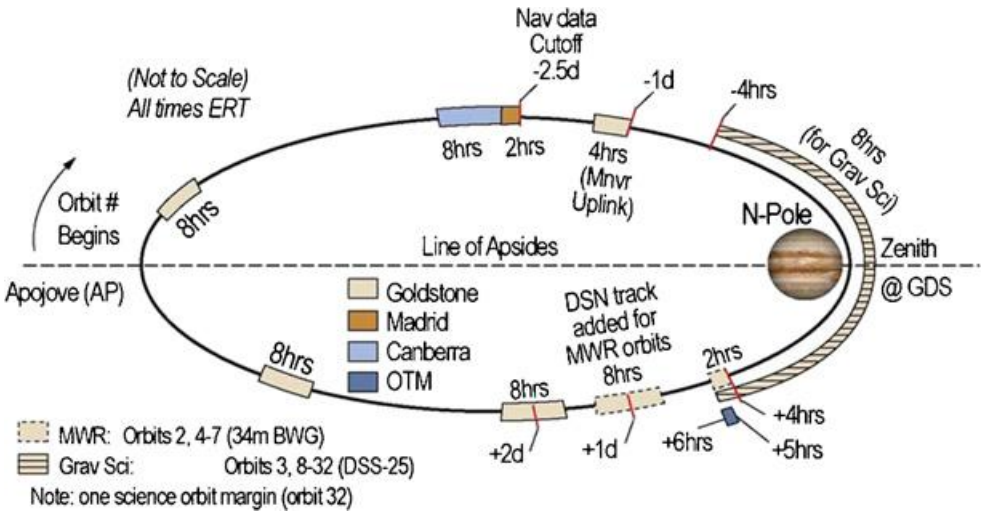

Figure 3.2.: Operations during the 32 orbits mission.

3.6 EXPECTATIONS FROM JUNO MISSION

In this section we try to make a quantitative prediction of the recoverability of Jupiter's gravity field by means of Juno mission.

In general, let us suppose to have a spacecraft in a nearly circular orbit at a constant altitude h above the surface of a planet with equatorial radius $R_\oplus$. By (2.9), the potential due to a spherical harmonic of degree ℓ and order m is given by

$$\frac{GM}{r}\left(\frac{R_\oplus}{r}\right)^{\ell}\overline{Y}_{\ell m1}\overline{C}_{\ell m}, \quad \frac{GM}{r}\left(\frac{R_\oplus}{r}\right)^{\ell}\overline{Y}_{\ell m0}\overline{S}_{\ell m},$$

where $r = R_\oplus + h$.
If we assume $h = \pi R_\oplus/\ell$, the *spatial scale of the harmonic of degree* ℓ, then the ratio of the monopole term GM/r to the harmonics with degree ℓ is

$$\left(\frac{R_\oplus}{r}\right)^{-\ell} = \left(\frac{R_\oplus + h}{R_\oplus}\right)^{\ell} = \left(1 + \frac{\pi}{\ell}\right)^{\ell} \xrightarrow[\ell\to+\infty]{} e^{\pi}.$$

We conclude that for high values of ℓ, the potential due to spherical harmonics of degree ℓ can be recovered worse than the monopole by a factor $e^\pi \simeq 23.14$. As h increases, say $h = k\pi R_\oplus/\ell$, this ratio becomes $e^{k\pi}$, making the gravity field signal decrease.

By looking at figure 3.3, which reproduces the 32 passages at perijove of the Juno probe, it is clear that the S/C flies over the northern emisphere at lower altitudes than over the southern emisphere. Thus, the sensitivity to higher-degree harmonics will be reduced in the latter, preventing from resolving correctly for the gravity field in this

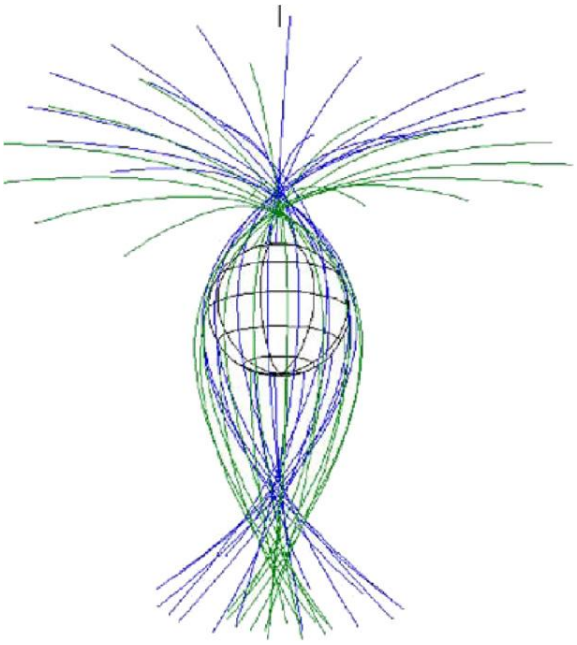

Figure 3.3.: Jupiter surface coverage by Juno spacecraft. The first 16 orbits are shown in blue, the second ones are shown in green.

zone of the planet. In conclusion, we expect a good recoverage of the gravitational potential at latitudes 11°N-33°N, corresponding to the perijoves of the Gravity Science experiment orbits, and a worse one for lower latitudes.

4

GRAVITY FIELD UNCERTAINTIES FROM JUNO MISSION

In this chapter we present the problem of determining the gravity field of a planet with a space mission involving an orbiter around the planet. Our aim is to study the formal error of the result with the tools of orbit determination recalled in chapter 1 and develop an analytic theory. We implement this theory in a MATLAB function which we use to study the case of the Juno mission to planet Jupiter. We give a description of the uncertainty of the zonal harmonic coefficients of Jupiter's gravitational potential in two cases: ignoring correlations with tesseral coefficients and taking them into account. We also perform a principal components analysis, from which we obtain the surface gravity anomalies uncertainties as function of the latitude, showing the surface portions where the gravity field can be well recovered.

4.1 RANGE AND RANGE-RATE

Probe tracking is an essential part of a space mission: measuring the distance and the velocity of a spacecraft is the mean by which gravity field mapping is possible. We can't help giving a solid mathematical model, in which distance and/or velocity measurements take into account corrections due to the general relativity theory and the movements of the planets.

If we choose an inertial frame centered in the Solar System Baricenter (SSB), we can express the vector $\mathbf{r}$ with origin at the ground antenna on Earth (e.g., the DSN) and pointing to a spacecraft orbiting another planet (e.g., the Juno probe around Jupiter) by (see figure 4.1)

$$\mathbf{r} = \mathbf{x}_{\mathrm{BJS}} + \mathbf{x}_{\mathrm{J}} + \mathbf{x}_{\mathrm{sat}} - \mathbf{x}_{\mathrm{E}} - \mathbf{x}_{\mathrm{ant}},$$

where:

- $\mathbf{x}_{\mathrm{BJS}}$ is the position of the Jovian System Barycenter;
- $\mathbf{x}_{\mathrm{J}}$ is the position of Jupiter's barycenter with respect to the BJS;
- $\mathbf{x}_{\mathrm{sat}}$ is the position of the spacecraft with respect to Jupiter's center of mass;
- $\mathbf{x}_{\mathrm{E}}$ is the position of the center of mass of the Earth;
- $\mathbf{x}_{\mathrm{ant}}$ is the position of the ground antenna with respect to the Earth center of mass.

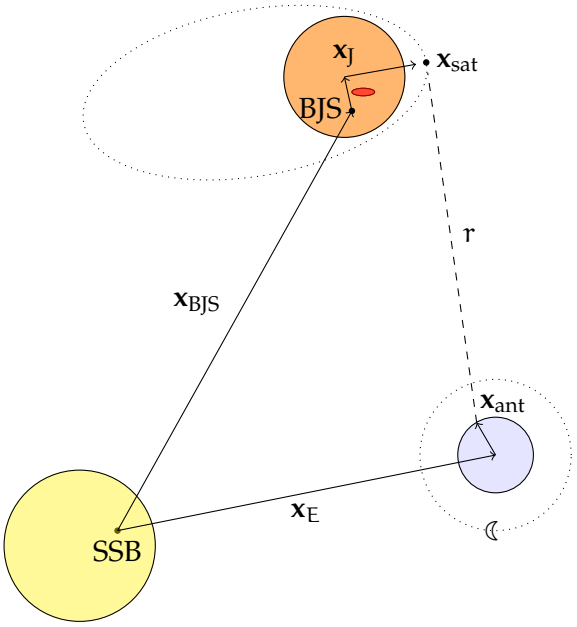

Figure 4.1.: A representation of the Sun/Earth/Jupiter system and relative distances. No scale has been used.

The *range* r of a spacecraft is its distance from the ground antenna, thus

$$r = |\mathbf{r}| + S(\gamma),$$

where $S(\gamma)$ is a correction due to the difference between the geodesics of the euclidean space and the ones of the curved space-time of general relativity, called *Shapiro effect*, depending upon the post-newtonian parameter γ. Actually, the signal from the spacecraft to the antenna on Earth travels at finite velocity, which is approximately c. It follows that during the propagation of the signal, the considered bodies move to a different position, making essential the definitions of three diverse instants of time: the transmission time t_t when the signal leaves the Earth, the bounce time t_b when it arrives at the spacecraft and comes back, and the receive time t_r when it gets back on Earth. Thus, we always have two distances: r_{up} and r_{down}, respectively relative to signal going from Earth to the probe and a signal going from the spacecraft to Earth. We then define $r := (r_{up} + r_{down})/2$.

The *range-rate* is the component of the velocity of the spacecraft along the direction of the Earth; in our notations, it has the following expression:

$$\dot{r} = \widehat{\mathbf{r}} \cdot \dot{\mathbf{r}} + \dot{S}(\gamma), \tag{4.1}$$

where

$$\dot{\mathbf{r}} = \dot{\mathbf{x}}_{BJS} + \dot{\mathbf{x}}_J + \dot{\mathbf{x}}_{sat} - \dot{\mathbf{x}}_E - \dot{\mathbf{x}}_{ant}$$

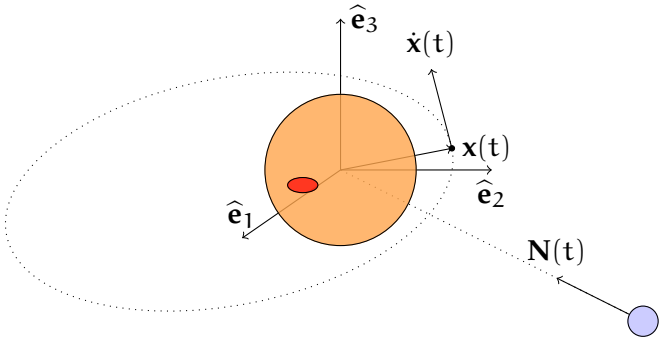

Figure 4.2.: The frame $O\widehat{\mathbf{e}}_1\widehat{\mathbf{e}}_2\widehat{\mathbf{e}}_3$, the spacecraft position and velocity $\mathbf{x}(t), \dot{\mathbf{x}}(t)$ and the direction Earth-Jupiter $\mathbf{N}(t)$. The vectors $\widehat{\mathbf{e}}_1, \widehat{\mathbf{e}}_2$ span the equatorial plane of the planet, the vector $\widehat{\mathbf{e}}_3$ is parallel to its rotation axis. The picture is not in scale.

holds the velocities of all the bodies involved. The same considerations we have done for the range are still valid: the propagation of the signal is not instantaneous, therefore we must introduce $\dot{r}_{down}, \dot{r}_{up}$, with expressions analogous to (4.1) and correct them to take into account the dependence of t_b, t_t on t_r. For further details about the dynamics affecting Juno's observables, see [11], for a deeper argumentation about the computation of the range-rate, see [10].

4.2 AXIAL SYMMETRIC PLANET

Let us consider a planet of mass M, equatorial radius R and symmetric with respect to the z-axis of an inertial frame $O\widehat{\mathbf{e}}_1\widehat{\mathbf{e}}_2\widehat{\mathbf{e}}_3$ of coordinates xyz, with origin in the center of mass of the planet, such that the xy plane is the equatorial plane of the planet (see figure 4.2).
The gravitational potential U of the planet is then function only of the latitude θ and the distance r from the center of mass. Thus, as seen in section 2.2, the expansion in spherical harmonics (2.4) only contains zonal coefficients:

$$U = \frac{GM}{r} + \sum_{\ell=2}^{\infty} U_\ell,$$

where

$$U_\ell = \frac{GM}{r} C_\ell \left(\frac{R}{r}\right)^\ell P_\ell(\sin\theta), \qquad \ell \geqslant 2.$$

Let $\ell_{max} > 2$ be an integer. We want to study the uncertainty with which the zonal harmonic coefficients $C_2, \dots, C_{\ell_{max}}$ can be determined. To do this, we use the tools of orbit determination recalled in chapter 1: indeed, the idea is to find analytical

expression for the elements of the normal matrix C.
Let the observation results be $(t_i, \nu_i)_{i=1,\dots,m}$, where ν_i is the range-rate of a spacecraft orbiting the planet. Let $\mathbf{x}(t)$ be the cartesian coordinates of the spacecraft at time t and $\dot{\mathbf{x}}(t)$ its velocity. Denote with $\mathbf{N}(t)$ the opposite of the unit vector pointing at the center of the Earth. Let's truncate the spherical harmonic expansion of U at degree ℓ_{max}. Note that by the *principle of linearity of the first order perturbations* (see A.3), we have

$$\dot{\mathbf{x}} = \mathbf{v} + \Delta\mathbf{v} = \mathbf{v} + \sum_{\ell=2}^{\ell_{max}} \Delta\mathbf{v}^{(\ell)},$$

where $\mathbf{v}$ is the component of the velocity due to the monopole

$$U_0 := \frac{GM}{r}$$

and $\Delta\mathbf{v}^{(\ell)}$ is the first order component due to the correction U_ℓ.

REMARKS 4.1 A. Among all the terms appearing in 4.1, only the spacecraft velocity depends on the gravity field of the planet. Indeed, the Earth's position and velocity are provided by the JPL ephemerides and Jupiter's position with respect to BJS is taken from the SPICE kernels of the Jovian system (see [6]). Therefore they can be treated as a known function of the time $w(t)$, not influencing the uncertainty of the result. In conclusion, the prediction function is

$$\nu(t) := \dot{\mathbf{x}}(t) \cdot \mathbf{N}(t) + w(t)$$

and therefore the residuals are

$$\xi_i = \nu_i - \nu(t_i) = \nu_i - \dot{\mathbf{x}}(t_i) \cdot \mathbf{N}(t_i) - w(t_i), \quad i = 1, \dots, m. \tag{4.2}$$

B. For an unperturbed orbit, energy (per unit of mass)

$$E := \frac{1}{2}|\mathbf{v}|^2 - U_0$$

is an integral of motion. Perturbing the gravitational potential with a term U_ℓ, the function

$$E_\ell := \frac{1}{2}|\mathbf{v} + \Delta\mathbf{v}^{(\ell)}|^2 - (U_0 + U_\ell)$$

is an integral of motion, equal to E. Thus

$$\frac{1}{2}|\mathbf{v}|^2 - U_0 = \frac{1}{2}|\mathbf{v} + \Delta\mathbf{v}^{(\ell)}|^2 - (U_0 + U_\ell)$$

and, neglecting second order terms,

$$\mathbf{v} \cdot \Delta\mathbf{v}^{(\ell)} = U_\ell \quad \text{for all } \ell.$$

In fact, the transversal component of $\Delta\mathbf{v}^{(\ell)}$ with respect to $\mathbf{v}$ is smaller than the parallel one, therefore we can suppose $\Delta\mathbf{v}^{(\ell)} \parallel \mathbf{v}$, the preeceding equation becoming

$$|\mathbf{v}||\Delta\mathbf{v}^{(\ell)}| = U_\ell \quad \text{for all } \ell. \tag{4.3}$$

In conclusion, a measurement of the range-rate of the spacecraft gives a direct measurement of the potential of the planet.

Combining the previous remarks, if φ_i is the angle between the vectors $\dot{\mathbf{x}}(t_i)$ and $\mathbf{N}(t_i)$, the residual assumes the expression

$$\begin{aligned}\xi_i &= \nu_i - (\mathbf{v}(t_i)\cdot\mathbf{N}(t_i) + \sum_\ell \Delta\mathbf{v}^{(\ell)}(t_i)\cdot\mathbf{N}(t_i)) - w(t_i)\\ &= \nu_i - (|\mathbf{v}(t_i)|\cos\varphi_i + \sum_\ell |\Delta\mathbf{v}^{(\ell)}(t_i)|\cos\varphi_i) - w(t_i).\end{aligned} \tag{4.4}$$

If $\boldsymbol{\mu} := (C_{\ell+1})_{\ell=1,\dots,\ell_{max}-1} \in \mathbb{R}^N$ is the vector of the fit parameters, we can build the design matrix $B = (b_{i\ell}) \in \mathbb{R}^{m\times N}$, where

$$b_{i\ell} = \frac{\partial\xi_i}{\partial\mu_\ell} = \frac{\partial\xi_i}{\partial C_{\ell+1}}.$$

By equation (4.3) and (4.4), we obtain

$$b_{i\ell} = -\frac{GM}{r_i}\left(\frac{R}{r_i}\right)^{\ell+1}\frac{P_{\ell+1}(\sin\theta_i)}{|\mathbf{v}_i|}\cos\varphi_i, \quad i = 1,\dots,m,\ \ell = 1,\dots,\ell_{max}-1, \tag{4.5}$$

where the subscript i indicates the evaluation in t_i.
Let $C := B^T W B = (c_{jk}) \in \mathbb{R}^{N\times N}$ be the normal matrix, where $W = s^{-2}I$ is the weight matrix; it immediately follows from the preceeding formula that

$$c_{jk} = \sum_{i=1}^{N} b_{ij}b_{ik} = \sum_{i=1}^{N}\frac{(GM)^2R^{j+k+2}}{r_i^{j+k+3}}\frac{P_{j+1}(\sin\theta_i)P_{k+1}(\sin\theta_i)}{s^2|\mathbf{v}_i|^2}\cos^2\varphi_i.$$

4.2.1 *Formal error and principal components analysis*

Let $\Gamma := C^{-1} = (\gamma_{ij})$ be the covariance matrix; by remark 1.19, the 1-σ *formal error* of each coefficient C_ℓ, $\ell = 2,\dots,\ell_{max}$, is the square root of the corresponding diagonal entry of the matrix Γ, i.e. $\sqrt{\gamma_{\ell-1\ell-1}}$.

We can predict the uncertainty of the *gravity anomalies*[1] on the surface of the planet with a principal components analysis. Let $\lambda_1 > \lambda_2 > \cdots > \lambda_N > 0$ be the eigenvalues of the covariance matrix Γ and let $V^{(i)} = (V_\ell^{(i)})_\ell$, $i = 1,\dots,N$ be respective

1 For us, a gravity anomaly is the difference between the real value of the gravity acceleration and the value due to the monopole term.

unit eigenvectors. It is a known fact that $\sqrt{\lambda_i}V^{(i)}$ is the i-th semiaxis of the 1-σ confidence ellipsoid, thus its entries are zonal harmonics coefficients. Consequently, each eigenvector $V^{(i)}$ can be mapped onto the following function:

$$U^{(i)}(r,\theta) := \frac{GM}{r}\sum_{\ell=2}^{\ell_{max}}\sqrt{\lambda_i}V^{(i)}_{\ell-1}\left(\frac{R}{r}\right)^{\ell}P_\ell(\sin\theta).$$

Each of the previous functions represents the contribute of the confidence ellipsoid's i-th semiaxis to the correction of U_0 due to harmonics of degrees $\ell = 2,\dots,\ell_{max}$. In other words, it is the uncertainty of the gravitational potential in the direction of the i-th semiaxis.

We can go on computing the radial component of the acceleration:

$$\frac{\partial U^{(i)}}{\partial r}(r,\theta) = -\frac{GM}{r^2}\sum_{\ell=2}^{\ell_{max}}(\ell+1)\sqrt{\lambda_i}V^{(i)}_{\ell-1}\left(\frac{R}{r}\right)^{\ell}P_\ell(\sin\theta), \quad i = 1,\dots,N;$$

by evaluating it in $r = R$, we obtain

$$\mathcal{U}^{(i)}(\theta) := \frac{\partial U^{(i)}}{\partial r}(R,\theta) = -\frac{GM}{R^2}\sum_{\ell=2}^{\ell_{max}}(\ell+1)\sqrt{\lambda_i}V^{(i)}_{\ell-1}P_\ell(\sin\theta), \quad i = 1,\dots,N \tag{4.6}$$

representing the uncertainty of the gravity anomalies on the surface of the planet due to the confidence ellipsoid's i-th semiaxis.
We use the *root mean square* of the $\mathcal{U}^{(i)}$ to have a representation of the surface acceleration uncertainty which takes into account the contributes from all the semiaxis:

$$\mathcal{U}(\theta) := \sqrt{\frac{\sum_{i=1}^{N}(\mathcal{U}^{(i)}(\theta))^2}{N}}. \tag{4.7}$$

If the magnitude of some $\mathcal{U}^{(i)}$ is negligible with respect to the others, we can choose not to consider it in the sum (4.7).

REMARK 4.2 - Note that the unit eigenvector relative to a certain eigenvalue is not unique: if $\mathbf{v}$ is such a vector, then also $-\mathbf{v}$ is. This causes an ambiguity in the definition of $U^{(i)}$, as it is defined except for the sign. This is not important as we are interested in $\mathcal{U}$, which doesn't see this ambiguity as in its expression only square powers of $\mathcal{U}^{(i)}$ appear.

4.3 EFFECT OF TESSERAL HARMONICS

Let us consider the same situation of section 4.2, this time without axial symmetry. The gravitational potential U of the planet, expressed in function of the distance r from the

center of mass, the latitude θ and the longitude λ, admits an expansion in spherical harmonics:

$$U(r,\theta,\lambda) = \frac{GM}{r} + \sum_{\ell=2}^{\infty}\sum_{m=0}^{\ell} U_{\ell m}$$

where

$$U_{\ell m} = \frac{GM}{r}\left(\frac{R}{r}\right)^{\ell} P_{\ell m}(\sin\theta)[C_{\ell m}\cos(m\lambda) + S_{\ell m}\sin(m\lambda)]. \tag{4.8}$$

Using the same notation as in section 4.2, the residual has the same expression (4.2). We now have to take into account the influence of tesseral harmonics, thus we use again the principle of linearity of the first order perturbations to write

$$\dot{\mathbf{x}} = \mathbf{v} + \Delta\mathbf{v} = \mathbf{v} + \sum_{\ell,m} \Delta\mathbf{v}^{(\ell,m)},$$

where $\mathbf{v}$ is the component of the velocity due to the monopole U_0 and $\Delta\mathbf{v}^{(\ell,m)}$ is the component due to the correction $U_{\ell m}$. An analogous argument to the one used in remark 4.1B allows us to conclude that

$$|\mathbf{v}||\Delta\mathbf{v}^{(\ell,m)}| = U_{\ell m} \quad \text{for all } \ell, m. \tag{4.9}$$

As before,

$$\begin{aligned}\xi_i &= \nu_i - (\mathbf{v}(t_i)\cdot\mathbf{N}(t_i) + \sum_{\ell,m}\Delta\mathbf{v}^{(\ell,m)}(t_i)\cdot\mathbf{N}(t_i)) - w(t_i)\\ &= \nu_i - (|\mathbf{v}(t_i)|\cos\varphi_i + \sum_{\ell,m}|\Delta\mathbf{v}^{(\ell,m)}(t_i)|\cos\varphi_i) - w(t_i),\end{aligned} \tag{4.10}$$

where φ_i is the angle between the vectors $\dot{\mathbf{x}}(t_i)$ and $\mathbf{N}(t_i)$.
Again, we want to study the uncertainty in the computation of the first ℓ_{max} zonal harmonic coefficients; if $\boldsymbol{\mu} \in \mathbb{R}^N$, $N := (\ell_{max}+1)^2 - 4$, is the vector of the fit parameters made up of both zonal and tesseral coefficients, we can build the design matrix $B = (\partial\xi_i/\partial\mu_j) \in \mathbb{R}^{m\times N}$ by combining equations (4.8), (4.9) and (4.10):

$$\frac{\partial\xi_i}{\partial C_{\ell m}} = -\frac{GMR^{\ell}}{r_i^{\ell+1}}\frac{P_{\ell m}(\sin\theta_i)}{|\mathbf{v}_i|}\cos(m\lambda_i)\cos(\varphi_i), \tag{4.11}$$

$$\frac{\partial\xi_i}{\partial S_{\ell m}} = -\frac{GMR^{\ell}}{r_i^{\ell+1}}\frac{P_{\ell m}(\sin\theta_i)}{|\mathbf{v}_i|}\sin(m\lambda_i)\cos(\varphi_i), \tag{4.12}$$

where the subscript i indicates the evaluation in t_i.

By reordering the entries of the vector $\boldsymbol{\mu}$, we can suppose that $\boldsymbol{\mu} = (\mathbf{z};\mathbf{t})$, where $\mathbf{z}$ is the subvector of the zonal harmonic coefficients and $\mathbf{t}$ is the subvector of the tesseral harmonic coefficients. We can perform an analogue analysis to the one shown in

section 1.3. The normal matrix C and the covariance matrix Γ have the block structure

$$C = \begin{pmatrix} C_{zz} & C_{zt} \\ C_{tz} & C_{tt} \end{pmatrix}, \quad \Gamma = \begin{pmatrix} \Gamma_{zz} & \Gamma_{zt} \\ \Gamma_{tz} & \Gamma_{tt} \end{pmatrix}, \tag{4.13}$$

where :

- the submatrices $\Gamma_{zt} = \Gamma_{tz}^T$ contain the correlations among zonal and tesseral coefficients;
- the submatrix C_{zz} is the normal matrix of the fit obtained by choosing $\mathbf{z}$ as vector of the fit parameters and moving $\mathbf{t}$ into the consider parameters, thus it is the same normal matrix of section 4.2.

The uncertainty of the zonal coefficients, considering correlations with tesseral coefficients, is given by Γ_{zz}, which has expression (see section 1.3)

$$\Gamma_{zz} = (C_{zz} - C_{zt}C_{tt}^{-1}C_{tz})^{-1}.$$

In brief, in order to compare the formal error in the computation of the zonal harmonic coefficients in the two cases, it suffices to compare the square root of the diagonal entries of the matrices C_{zz}^{-1} and Γ_{zz}.

4.4 JUPITER CASE

In this section we apply the theory developed in the previous sections to planet Jupiter. What we want to do is studying the formal error committed in determining Jupiter's harmonic coefficients with Juno mission. First we suppose Jupiter being axial symmetric, then we complete the study taking into account correlations with tesseral coefficients. We also give a prediction of gravity anomalies accuracy on the surface of the planet, in order to have an idea of how well the gravity field can be recovered at different latitudes. We repeat this analysis twice: using a single simulated passage at perijove of Juno probe, namely the one belonging to orbit 8, and then using a simulation of all the passages at perijove destined to Gravity Science experiment, from orbit 8 to 32.

4.4.1 *Description of the algorithm*

We implemented the theory described in section 4.2 in a MATLAB function called `uncertainties`. The user is invited to specify a value for ℓ_{max}, the highest degree in the truncation of the spherical harmonics series of Jupiter's potential U.
The algorithm reads datas from 25 simulated passages[2] at perijove of Juno probe,

2 The arcs have been provided by the `orbit14` Juno simulator program.

the ones destined to Gravity Science experiment. Each passage is composed of 721 30-seconds-spaced observations and include positions and velocities of the spacecraft $(\mathbf{x}(t_i))_i$, $(\dot{\mathbf{x}}(t_i))_i$ and unit vectors along the direction of the Earth $(\mathbf{N}(t_i))_i$. All the observations are referred to a frame $O\hat{\mathbf{e}}_1\hat{\mathbf{e}}_2\hat{\mathbf{e}}_3$ with origin at Jupiter's center of mass, with $\hat{\mathbf{e}}_1\hat{\mathbf{e}}_2$ spanning the equatorial plane and $\hat{\mathbf{e}}_3$ pointing at the North pole.
The algorithm converts the observations to spherical coordinates using the inverse transformation of (2.2). Design matrix B is computed according to (4.5), in a form that involves normalized spherical harmonics, which are numerically convenient:

$$b_{i\ell} = -\frac{GM}{r_i}\left(\frac{R}{r_i}\right)^{\ell+1}\frac{\overline{Y}_{\ell+101}(\sin\theta_i)}{|\mathbf{v}_i|}\cos\varphi_i, \quad i = 1,\dots,m,\ \ell = 1,\dots,\ell_{max}-1;$$

with this choice, the procedure will give as result the uncertainty of $\overline{C}_\ell = \sqrt{2\ell+1}C_\ell$. The performance of the KaT (Ka-band Trasponder) of Juno spacecraft is of 3×10^{-4} cm/s on an integration time of 1000 s. By gaussian statistics, as the observations are 30-seconds spaced, we give a uniform weight $s := \sqrt{1000/30}\ 3\times10^{-4}$cm/s to all the observations, introducing a weight matrix $W := s^{-2}I$. The algorithm computes the normal matrix $C := \sigma^{-2}B^TB$, its inverse Γ and plots the square roots of its diagonal entries.

The principal components analysis is performed as described in section 4.2.1. The eigenvalues and eigenvectors of Γ are computed and the uncertainty of gravity anomalies is obtained implementing formula (4.6), using normalized Legendre polynomials $\overline{P}_\ell$.

The following constant values are assumed known from other space missions: $R_{♃} = 7.1492\times10^4$ km for Jupiter's equatorial radius, $GM_{♃} = 1.2674\times10^8$ km^{3}s^{-2}.

4.4.2 *Analysis of the results*

We executed the algorithm twice: the first time considering datas from a single passage at perijove (orbit 8), the second one with a complete 25 passages mission. Both the times we chose $\ell_{max} = 40$.

FORMAL ERROR Figure 4.3 shows the uncertainty of the normalized zonal harmonic coefficients $\overline{C}_\ell$ resulted from the two executions. It is no surprise that the formal error is minor when a complete 25 arcs mission is considered, as more observations result in more accuracy. However, this estimate cannot be considered realistic, as it has been computed ignoring correlations with tesseral harmonic coefficients, which we will consider in section 4.4.3. It's interesting to remark that the uncertainties don't always increase: they reach the maximum value at degree 29, then they decrease. This behaviour is due to the fact that each zonal coefficient is correlated to the following one: truncating the spherical harmonics series at degree 40 is the same as introducing the constraint on the zonal

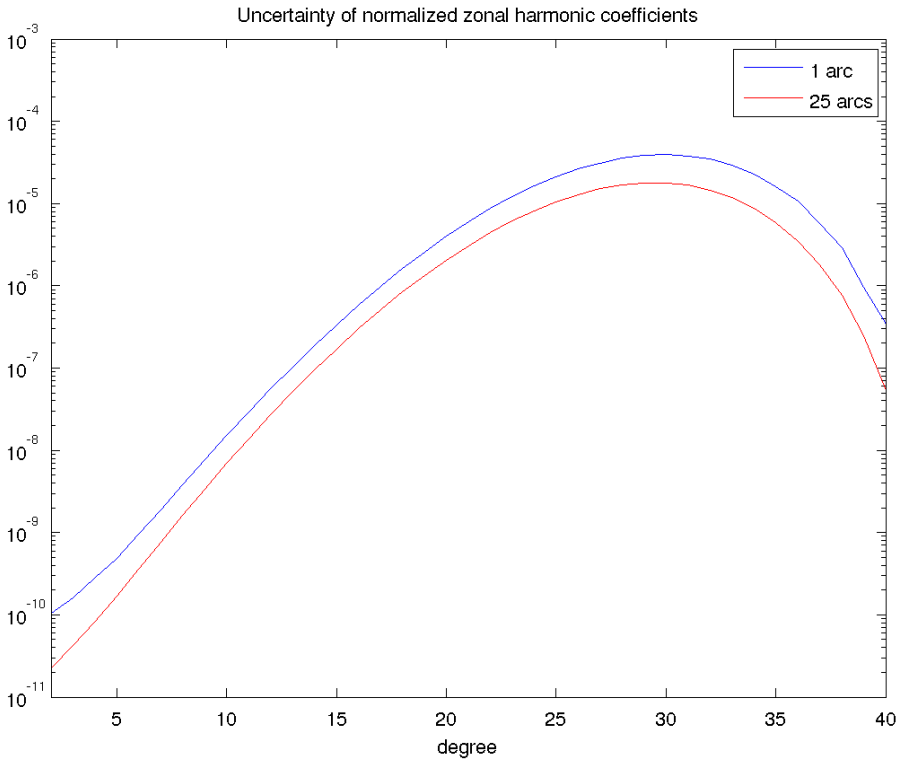

Figure 4.3.: Formal errors of the first 40 zonal harmonic coefficients in Jupiter's potential, computed with 1 passage and 25 passages at perijove. Semilogarithmic scale is used.

coefficients to be a finite number, thus the last one will be correlated only to the previous coefficents, causing a diminution of the uncertainty for the highest degrees coefficients. This "hump" behaviour doesn't depend on the particular value of ℓ_{max}, of course.

PRINCIPAL COMPONENTS ANALYSIS Figure 4.4a shows the square root of the eigenvalues of the covariance matrix Γ in the two examined cases. It is clear that $\sqrt{\lambda_1}, \sqrt{\lambda_2}$ are much bigger than the others, therefore we could expect that their effect on the surface gravity anomalies uncertainty is dominating.
Actually, this is only partially true. To understand this, it is useful to look at figure 4.4b: here the contributes due to $\sqrt{\lambda_i}V^{(i)}$, $i = 2, 10, 20, 30$ are compared with the effect of $\sqrt{\lambda_1}V^{(1)}$ (we considered the 25 passages case, but the same deductions can be made from the other one). The effect on the polar caps rapidly

decreases as i grows[3], while the effect on middle latitudes, especially around the perijove, is substantially the same in order of magnitude up to $i = 20$. For $i > 20$, even this effect can be considered negligible as the corresponding figure for $i = 30$ suggests.
Thus, in order to describe Jupiter's surface acceleration uncertainties, we compute the root mean square of $\mathcal{U}^{(i)}$ (4.7), $i = 1, \dots, 20$. The result is shown in figure 4.5: in both cases the gravity field at the South pole is badly recovered, as the uncertainty at lowest latitudes is $> 10^4$ mGal. On the contrary, the gravity field at latitudes corresponding to the perijoves ($\simeq 11°$N to $\simeq 34°$N) is well determined. As the wider "belly" of the red plot suggests, a complete mission permits a better mapping rather than a single passage, of course. It is evident that this result heavily depends on the geometry of the orbit of the Juno spacecraft, for instance the latitude of the pericenter. As we will see in the next subsection, when we will study the influence of the tesseral coefficients on the uncertainty, this is substantially the main element affecting the gravity anomalies accuracy predictions.

4.4.3 *Correlations with tesseral coefficients*

We modified the algorithm `uncertainties` in accordance to section 4.3 in order to take into account correlations with tesseral spherical harmonics. In this case the analysis can be done only with the datas coming from all the 25 arcs, otherwise the fit parameters would be more than the observations, making the recovering impossible.

If $\boldsymbol{\mu}$ is the vector of the fit parameters, we use the ordering

$$\begin{cases} C_{\ell m} = \mu_{\ell^2+2m-3} & \ell \geqslant 2,\ 0 \leqslant m \leqslant \ell \\ S_{\ell m} = \mu_{\ell^2+2m-4} & \ell \geqslant 2,\ 1 \leqslant m \leqslant \ell \end{cases}$$

and formulæ(4.11) to compute the design matrix B (normalized Legendre associated functions are utilized to avoid overflow problems). Noting that the zonal harmonic coefficients are in the subvector $\mathbf{z} := (\mu_{\ell^2-3})_{\ell \geqslant 2}$, `uncertainties` reorders the columns of B so that

$$B = \left(\frac{\partial \xi}{\partial \mathbf{z}}, \frac{\partial \xi}{\partial \mathbf{t}} \right),$$

where $\mathbf{t}$ is the vector of the tesseral coefficients, and $C = s^{-2} B^T B$, Γ have expressions (4.13).

We already remarked that the formal error of the zonal coefficients, comprehensive of tesseral harmonics correlations, is given by the diagonal entries of

$$\Gamma_{\mathbf{zz}} = (C_{\mathbf{zz}} - C_{\mathbf{zt}} C_{\mathbf{tt}}^{-1} C_{\mathbf{tz}})^{-1}.$$

3 This is evident already for $i = 2$: the effect on the South pole is 2 orders of magnitude smaller.

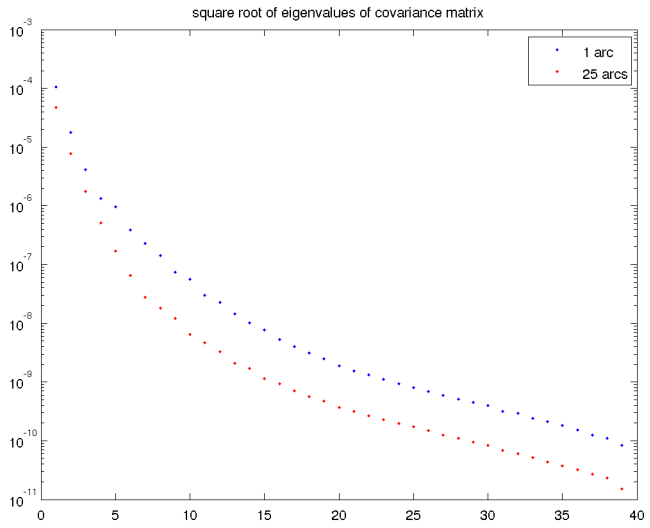

(a) Square root of eigenvalues of covariance matrix Γ, in the case of one passage and two passages (semilogarithmic scale).

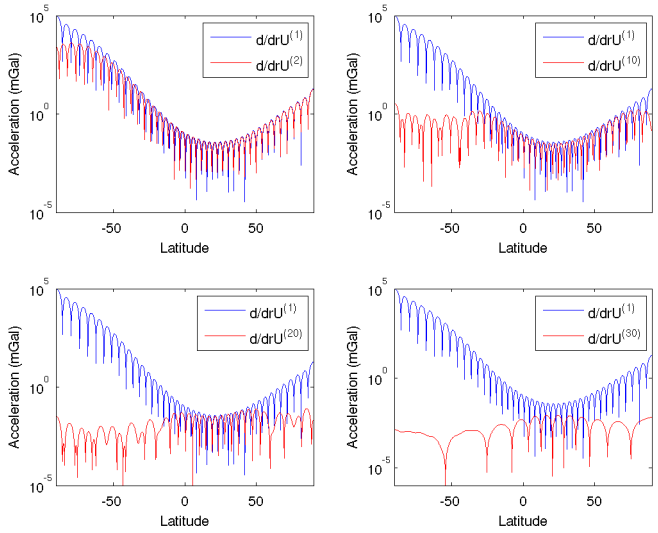

(b) Comparison between gravity anomalies uncertainty due to $\sqrt{\lambda_1}V^{(1)}$ and $\sqrt{\lambda_i}V^{(i)}$, $i = 2, 10, 20, 30$ (25 passages have been used). The difference in magnitudine between eigenvalues reflects into a difference in anomalies uncertainty on polar caps, while around the perijove their influences are the same in terms of order of magnitude, at least up to $i = 20$.

Figure 4.4.: Study of the surface gravity anomalies uncertainties

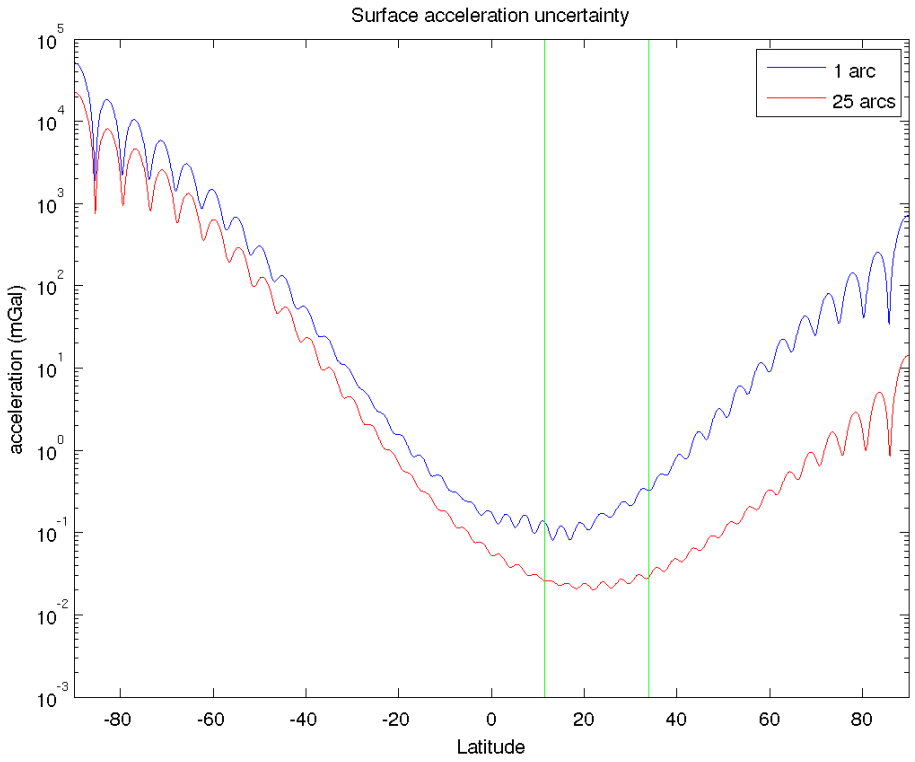

Figure 4.5.: Root mean square of $u^{(i)}$, $i = 1, \ldots, 20$, in both the cases considered, plotted in semilogarithmic scale; the green lines bound the perijove latitude band of Juno probe's 25 Gravity Science orbits.

It happens that the computation of the latter is difficult because the matrix C_{tt} is badly conditioned ($\mathrm{cond}(C_{tt}) \simeq 5 \times 10^{23}$ in norm 1). We can avoid this obstacle by adding some a priori observations of the tesseral coefficients, as described in section 1.4: according to some existing models of Jupiter's gravity field, we can suppose that the tesseral coefficients aren't bigger than 10^{-8}, that is we can assume we observed Jupiter's potential tesseral coefficients being $t_P := 0$ with uncertainty $\pm\sigma_P = \pm 10^{-8}$ and add to C_{tt} the a priori normal matrix $C_P := \sigma_P^{-2} I$, where I is the identity matrix of the suitable dimension. The new covariance matrix is

$$\Gamma_{zz} = [C_{zz} - C_{zt}(C_{tt} + C_P)^{-1} C_{tz}]^{-1},$$

which is no more badly conditioned. In figure 4.6 the result is compared to the formal error obtained ignoring tesseral harmonics. While the uncertainty is quite higher for low-degree coefficients, it is almost the same for high-degree ones. This confirms the fact that the accuracy with which the zonal harmonic coefficients can be recovered

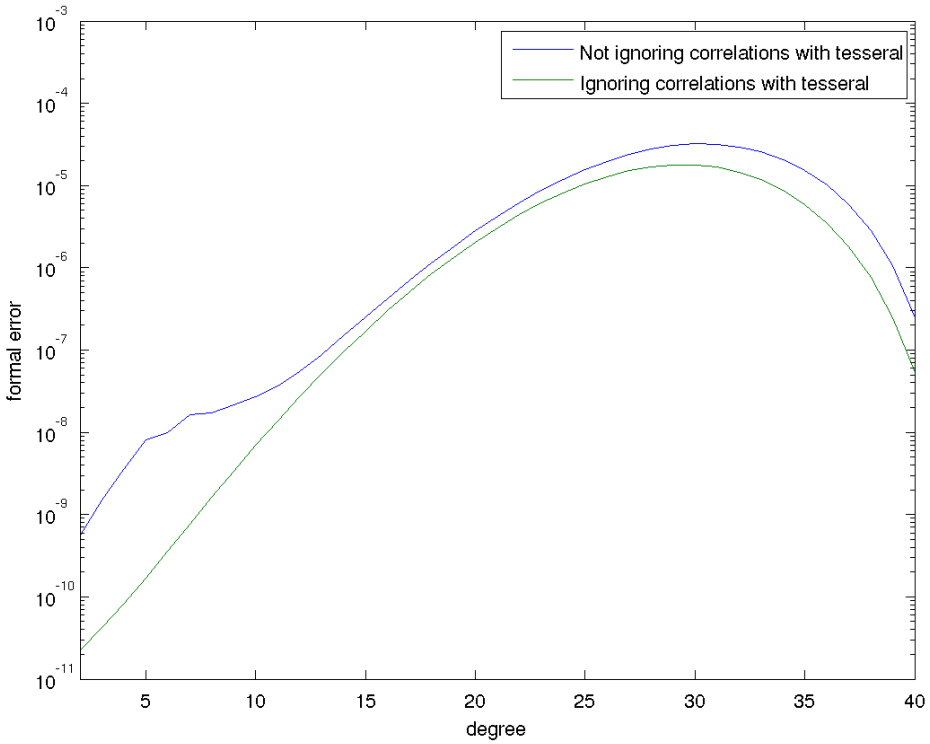

Figure 4.6.: Formal errors in the computation of the zonal harmonic coefficients of Jupiter's gravitational potential expansion in spherical harmonics. One curve is obtained neglecting correlations with tesseral coefficients, the other one considering them.

does not depend on external factors, e.g. the tesseral harmonic coefficients, but mainly on the spacecraft's orbit geometry.

4.5 COMPARISON WITH OTHER WORKS

The *Radio Science Laboratory* (RSL), University of Rome "La Sapienza", worked on numerical simulations of the Juno mission Gravity Science Experiment using the NASA's Orbit Determination Program (ODP), whose executable file was made available by the Jet Propulsion Laboratory[4]. They performed an orbit determination simulation and gave estimation of the uncertainty of the zonal harmonic coefficients and of the surface acceleration uncertainty. We compare our results, largely described in section 4.4,

4 Note that the source file cannot be exportated, so the RSL could not acceed to it.

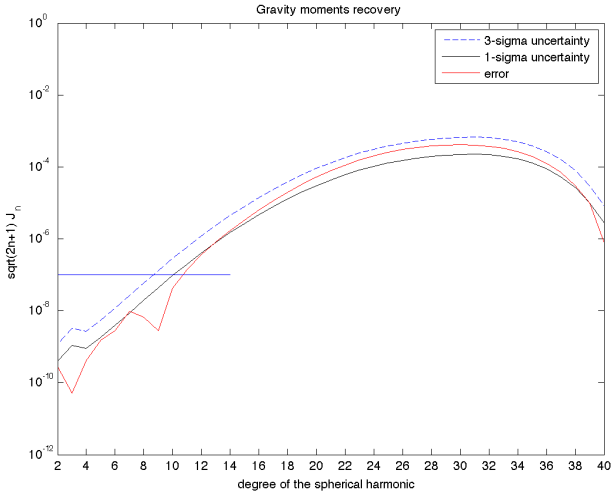

(a) Formal error of the normalized zonal harmonic coefficients from *Radio Science Lab*. The 1-σ and 3-σ curves are plotted, compared with the effective error resulted from a simulation. The horizontal segment shows the mission requirements.

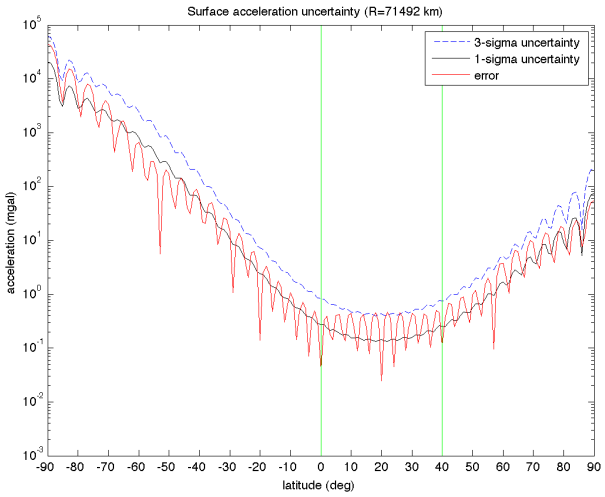

(b) Surface acceleration uncertainty as function of the latitude from *Radio Science Lab*. The 1-σ and 3-σ curves are plotted, compared with the effective error resulted from a simulation. The vertical green lines bound the latitudes of good spatial reconstruction, corresponding to the latitudes of the perijoves.

Figure 4.7.: *Radio Science Laboratory*'s results

with RSL's ones, presented at the Juno Science Team Meeting at Cocoa Beach (FL) on July, 2011.

ZONAL HARMONICS UNCERTAINTIES The black curve in figure 4.7a is the 1-σ uncertainty of the zonal harmonic coefficients, not considering correlations with tesserals, obtained by RSL. We compare it with our predictions of figure 4.3, red line. It is clear that the two results are qualitatively the same, as the maximum values are reached approximately at the same degree and so the minimum values. Nevertheless, our accuracy predictions are smaller, the difference being of one order of magnitude.

SURFACE ACCELERATION UNCERTAINTIES We compare figure 4.7b, the surface gravity uncertainty obtained by Rome team, with our results (figure 4.5, red plot). The qualitative behaviour of the two curves is clearly the same. They both reach the minimum value around latitude 20°N, but ours is 5 times smaller. The value at the North pole we have obtained is 3.5 times smaller than RSL's. Finally, the maximum values, obtained in both cases at the South pole, are identical.

In general, our results are more optimistic. This may be due to many causes: first, the RSL team used *a priori* observations of the zonal coefficients C_2, C_4, C_6 as given in [2] and the a priori value 0 ± 10^{-5} for all the other normalized zonal coefficients; second, a different weight matrix has been chosen. Another source of diversity is that the Rome team obtained its results from an orbit determination simulation. They do not only determine the zonal coefficients, but also the initial conditions of the spacecraft (6 parameters per passage). This introduces new correlations in the model, which make the uncertainty increase.
In general, it is not difficult to obtain differences of one order of magnitude in the outcomes of two different simulations: it is enough to choose different weights or different a priori oservations. On the contrary, such differences don't afflict the predictions about the latitudes at which the gravity field is well recovered, and the comparison between figures 4.7b and 4.5 confirms this. Such predictions are an intrinsic factor of the space mission, that is they are established by the orbit of the spacecraft. The consequence is simple: determining Jupiter's gravity field with good accuracy on a wider latitude band can only be achieved by changing the orbit. The latter is not a simple operation, as the orbit of the probe is chosen by taking other factors into account, such as the planet environment or the other experiments' requirements. In conclusion, the chosen orbit is always the compromise among the success of the gravity experiment, the desire of carrying out as many experiments as possible and the necessity to have a working spacecraft at disposal until the end of the mission.

CONCLUSIONS AND FUTURE WORK

We have developed a semi-analytic theory for the study of the uncertainty of Jupiter's gravitational potential zonal harmonic coefficients recovered with the NASA Juno mission. The method we have described is very simple and has been easily implemented in a MATLAB function. In particular, all we needed to obtain our results was a simulation of the spacecraft's orbit around Jupiter, provided by the `orbit14` Juno simulator program.
We have also compared our predictions with the results of some numerical simulations of the Juno mission Gravity Science experiment made by the *Radio Science Laboratory* in Rome. We have outlined that our outcome is quite more optimistic than the other team's: this may be due to some difference in the sampling of the orbit, in the a priori uncertainties or in the weight matrix. Moreover, since they performed an orbit determination simulation, their accuracy predictions may be affected by correlations with other parameters, such as the initial conditions of the spacecraft or possibly the non-gravitational perturbations. Nevertheless, the two results are qualitative the same, showing that the main factor influencing the uncertainty predictions is the spacecraft's orbit geometry, for instance its position with respect to a jovicentric frame, and the latitudes covered by the perijove passages.

A possible development of our work is to test `uncertainties` on accomplished interplanetary missions, whose results have been published. For instance, it would be interesting to consider the case of NASA's MeSSEnGeR mission to Mercury, which was characterized by a highly eccentric orbit, with a 200 km-altitude perihermion covering latitudes from 60°N to 72°N, and a 15200 km apohermion altitude; the consequent lack of sensitivity to higher degree harmonics in the southern hemisphere has caused a poor recovering of Mercury's gravity field in this zone, as described in [8]. Another source of interest are old lunar missions, like NASA's Lunar Prospector, which provided a good recovering of the Moon's gravity field on the near side, but could not give good solutions for the far side, due to the impossibility of tracking the probe in this zone.

After this phase of testing our theory, a possible research project may contemplate the planning of the architectural structure and the consequent implementation of a more sophisticated software based on our function `uncertainties`. For instance, this program could take as input values an integer ℓ_{max}, the mass and the equatorial radius of a planet and a sampling of the orbit of a spacecraft around it; it would provide a prediction, possibly optimistic, of the uncertainties obtained when solving for ℓ_{max} zonal harmonic coefficients of the planet's gravitational potential with a Gravity Science ex-

periment characterized by such an orbit. This software may become a useful tool to be used in a preliminary phase of a space mission design. Indeed, the mission scientific objectives, in order to ensure good accuracy in the outcome of the experiment, often require the determination of the zonal harmonic coefficients with an a priori established uncertainty. As we have seen in chapter 3, this is the case of Juno mission, which requires a good knowledge of coefficients C_2, C_4, C_6 to constrain Jupiter's core mass and of coefficients C_8 to C_{14} to determine the depth of the zonal winds. Our software may help discard the "bad" orbits, that is the ones causing a low accuracy, and may select all the orbits for which the uncertainty of the solution is below the limit.

This thesis points out a trivial, but fundamental fact about gravity field determination: it heavily depends on the chosen orbit for the spacecraft. The teaching we can learn is simple: strange behaviours of the gravity field on bad-observed zones of a celestial body should be no source of surprise, they are perfectly justified by the lack of sensitivity of the spacecraft. With this in mind, a surprisingly perfect X-shaped gravity anomaly on the far side of the Moon should not be considered the proof of the existence of an alien base, rather as the consequence of absent communication with the spacecraft in that zone of our natural satellite.

A

TOOLS FROM CELESTIAL MECHANICS

In this appendix we list and briefly describe some important instruments from Celestial Mechanics we have used throughout the thesis.

A.1 KEPLERIAN ELEMENTS

Let's consider the motion of a satellite in a planet gravity field. If the gravitational potential is keplerian, that is

$$U = U_0 = \frac{GM}{r},$$

where M is the mass of the planet and r is the distance from the planet's center of mass, then the orbit of the satellite is a conic section and can be described by six orbital elements, also called *keplerian elements*. In the case of closed orbit, it is an ellipse and the keplerian elements are the *semimajor axis* a, the *eccentricity* e, the *inclination* I of the orbit with respect to the equatorial plane of the planet, the *longitude of the ascending node* Ω and the *argument of pericenter* ω (see figure 2.1 for a visual description) and the *true anomaly* ν, the angle between the direction of the pericenter given by the Lenz vector $\mathbf{e}$ and the position of the satellite. Sometimes the latter is replaced by the *mean anomaly* $l = n(t - t_0)$, where t_0 is some starting time and n is the *mean motion*, related to a by Kepler's third law

$$n^2 a^3 = GM.$$

The keplerian elements are all constant except for ν (see [7], chapter 4, for further details).

A.2 THE LAGRANGE PLANETARY EQUATION FOR ω

If the potential is not keplerian, but it is perturbed for instance by some $U_{\ell m}$ term of Kaula's expansion (2.10), then the motion can still be described by means of the orbital elements above, but they're no more constant. It is not our aim to give a complete description of the variation of the orbital elements in presence of a perturbative term, we limit ourselves to write and comment the equations for the variation of the argument of pericenter ω.
Let us suppose the potential is $U = U_0 + R$, where R is a perturbing term. The equation of motion for ω is

$$\frac{d\omega}{dt} = \frac{\sqrt{1-e^2}}{na^2 e}\frac{\partial R}{\partial e} - \frac{\cot I}{na^2\sqrt{(1-e^2)}}\frac{\partial R}{\partial I},$$

which is called *Lagrange planetary equation* for the argument of pericenter.

EXAMPLE A.1 - Let us suppose $R = U_{20}$. From Kaula's expansion, we have

$$U_{20} = \frac{GMR_{\oplus}^2}{a^3} C_{20} \sum_{p=0}^{2} F_{20p}(I) \sum_{q} G_{\ell pq}(e) \cos[(2-2p)\omega + (2-2p+q)l]. \tag{A.1}$$

We are interested in the *secular perturbations*: intuitively, they are due to terms of the perturbing potential which are not periodic or to periodic terms with a period $P \gg T$, the orbital period of the spacecraft. Thus, we do not consider the terms containing l, as they give arise to *short-period* perturbations. It's easy to see that the only interesting term in (A.1) is

$$U_{2010} = \frac{GMC_2R_{\oplus}^2}{a^3} F_{201}(I) G_{210}(e),$$

where

$$F_{201}(I) = \frac{3}{4}\sin^2 I - \frac{1}{2}, \quad G_{210}(e) = (1-e^2)^{-\frac{3}{2}}.$$

By omitting some easy passages, we obtain

$$\frac{d\omega}{dt} = -\frac{3C_2R_{\oplus}^2 n}{a^2(1-e^2)^2}\left(1 - \frac{5}{4}\sin^2 I\right).$$

For a satellite on a polar orbit, it is evident that if $C_2 < 0$, then $\dot{\omega} > 0$, causing the increasing of the latitude of the pericenter.

A.3 FIRST ORDER PERTURBATIONS

Let us suppose we have a *perturbated dynamical system*

$$\dot{\mathbf{y}}(t) = \mathbf{F}_0(\mathbf{y}) + \epsilon \mathbf{F}_1(\mathbf{y}), \tag{A.2}$$

where the perturbation is of order of ϵ; we can write the general solution as

$$\mathbf{y}(t, \epsilon) = \mathbf{y}_0(t) + \epsilon \mathbf{y}_1(t) + \epsilon^2 \mathbf{y}_2(t) + \dots. \tag{A.3}$$

We want to study the properties of $\mathbf{y}_0, \mathbf{y}_1, \dots$; to do this, we start finding the differential equations they solve.
Replace (A.3) in (A.2):

$$\dot{\mathbf{y}}_0(t) + \epsilon\dot{\mathbf{y}}_1(t) + \epsilon^2\dot{\mathbf{y}}_2(t) + \dots = \mathbf{F}_0(\mathbf{y}) + \epsilon\mathbf{F}_1(\mathbf{y}),$$

then expand $\mathbf{F}_0, \mathbf{F}_1, \dots$ around $\mathbf{y}_0$:

$$\mathbf{F}_0(\mathbf{y}) = \mathbf{F}_0(\mathbf{y}_0) + \epsilon \frac{\partial \mathbf{F}_0}{\partial \mathbf{y}}(\mathbf{y}_0)\mathbf{y}_1 + \dots$$

$$\mathbf{F}_1(\mathbf{y}) = \mathbf{F}_1(\mathbf{y}_0) + \epsilon \frac{\partial \mathbf{F}_1}{\partial \mathbf{y}}(\mathbf{y}_0)\mathbf{y}_1 + \dots$$

$$\dots$$

Finally, equal the terms of the same order in ϵ:

$$\dot{\mathbf{y}}_0(t) = \mathbf{F}_0(\mathbf{y}_0)$$
$$\dot{\mathbf{y}}_1(t) = \frac{\partial \mathbf{F}_0}{\partial \mathbf{y}}(\mathbf{y}_0)\mathbf{y}_1 + \mathbf{F}_1(\mathbf{y}_0) \tag{A.4}$$
$$\dots \tag{A.5}$$

In particular, the first order equations are linear, thus the so-called *principle of linearity of the first order perturbations* follows: when we want to compute the first order solutions of a perturbated dynamical system

$$\dot{\mathbf{y}}(t) = \mathbf{F}_0(\mathbf{y}) + \epsilon \sum_{\ell=1}^{L} \mathbf{F}_\ell(\mathbf{y}),$$

we can independently solve for the first order solutions of the L dynamical systems

$$\dot{\mathbf{y}}(t) = \mathbf{F}_0(\mathbf{y}) + \epsilon \mathbf{F}_\ell(\mathbf{y}), \quad \ell = 1, \dots, L,$$

which are given by (A.4), and then sum them all.

BIBLIOGRAPHY

[1] E. Heine. *Handbuch der Kugelfunctionen. Theorie und Anwendungen. Band I, II*. Zweite umgearbeitete und vermehrte Auflage. Thesaurus Mathematicae, No. 1. Würzburg, 1961: Physica-Verlag, 1961, Band I:xvi+484 pp.; Band II:xii+380.

[2] R. A. Jacobson. *The JUP230 orbit solution*. 2003.

[3] William M. Kaula. *Theory of satellite geodesy: applications of satellites to geodesy*. Dover Earth Science Series. Dover Publications, 1966. ISBN: 9780486414652.

[4] Steve Matousek. "The Juno New Frontiers mission". In: *Acta Astronautica* 61.10 (2007), pp. 932 –939. ISSN: 0094-5765. DOI: 10.1016/j.actaastro.2006.12.013. URL: http://www.sciencedirect.com/science/article/pii/S0094576507000124.

[5] Andrea Milani and Giovanni F. Gronchi. *Theory of orbit determination*. Cambridge: Cambridge University Press, 2010, pp. x+382. ISBN: 978-0-521-87389-5.

[6] *NAIF CSPICE Toolkit Hypertext Documentation*. URL: http://naif.jpl.nasa.gov/pub/naif/toolkit_docs/C/index.html.

[7] Archie E. Roy. *Orbital motion*. Halsted Press [John Wiley & Sons], New York, 1978, pp. xiv+489. ISBN: 0-470-99251-4.

[8] David E. Smith et al. "Gravity Field and Internal Structure of Mercury from MESSENGER". In: *Science* 336.6078 (2012), pp. 214–217. DOI: 10.1126/science.1218809. eprint: http://www.sciencemag.org/content/336/6078/214.full.pdf. URL: http://www.sciencemag.org/content/336/6078/214.abstract.

[9] Elias M. Stein and Guido Weiss. *Introduction to Fourier analysis on Euclidean spaces*. Princeton Mathematical Series, No. 32. Princeton, N.J.: Princeton University Press, 1971, pp. x+297.

[10] G. Tommei, A. Milani, and D. Vokrouhlický. "Light-time computations for the BepiColombo Radio Science Experiment". In: *Celestial Mech. Dynam. Astronom.* 107.1-2 (2010), pp. 285–298. ISSN: 0923-2958. DOI: 10.1007/s10569-010-9273-7. URL: http://dx.doi.org/10.1007/s10569-010-9273-7.

[11] G. Tommei et al. *Orbit determination for the Radio Science experiment of the NASA mission Juno*. Proceeding of International Astronautical Congress 2012, available on CD-ROM. Naples.